INVESTIGATION OF MOLECULAR PROPERTIES OF HEAVY METAL DOPED GRAPHENE AND FORMATION FROM PYRENE USING DENSITY FUNCTIONAL THEORY

2024
PhD THESIS
PHYSICS

Lina Majeed Haider AL-HAIDERI

Thesis Advisor
Prof. Dr. Necla ÇAKMAK

INVESTIGATION OF MOLECULAR PROPERTIES OF HEAVY METAL DOPED GRAPHENE AND FORMATION FROM PYRENE USING DENSITY FUNCTIONAL THEORY

Lina Majeed Haider AL-HAIDERI

Thesis Advisor
Prof. Dr. Necla ÇAKMAK

T.C.
Karabük University
Institute of Graduate Programs
Department of Physics
Prepared as
PhD Thesis

KARABÜK
January 2024

I certify that in my opinion the thesis submitted by Lina Majeed Haider Al- HAIDERI titled "INVESTIGATION OF MOLECULAR PROPERTIES OF HEAVY METAL DOPED GRAPHENE AND FORMATION FROM PYRENE USING DENSITY FUNCTION THEORY" is fully adequate in scope and in quality as a thesis for the degree of PhD.

Prof. Dr. Necla ÇAKMAK .....

Thesis Advisor, Department of Physics

This thesis is accepted by the examining committee with a unanimous vote in the Department of Physics as a PhD thesis. Jan 30, 2024

Examining Committee Members (Institutions)	Signature
Chairman : Prof. Dr. Şeref TURHAN (KU)	.....
Member : Prof. Dr. Aybaba HANÇERLİOĞULLARI (KU)	.....
Member : Prof. Dr. Rıdvan BALDIK (ZBEU)	.....
Member : Prof. Dr. Necla ÇAKMAK (KBU)	.....
Member : Assoc. Prof. Dr. Ahmet Mustafa ERER (KBU)	.....

The degree of PhD by the thesis submitted is approved by the Administrative Board of the Institute of Graduate Programs, Karabük University.

Assoc. Prof. Dr. Zeynep ÖZCAN .....

Director of the Institute of Graduate Program

"I declare that all the information within this thesis has been gathered and presented in accordance with academic regulations and ethical principles and I have according to the requirements of these regulations and principles cited all those which do not originate in this work as well."

Lina Majeed Haider Al- HAIDERI

ABSTRACT

Ph.D.

INVESTIGATION OF MOLECULAR PROPERTIES OF HEAVY METAL DOPED GRAPHENE AND FORMATION FROM PYRENE USING DENSITY FUNCTIONAL THEORY

Lina Majeed Haider Al- HAIDERI

Karabük University
Institute of Graduate Programs
Department of Physics

Thesis Advisor:
Prof. Dr. Necla ÇAKMAK
Jan 2024, 65 pages

In this study, coronene regarded as an exemplary structure of graphene at a molecular level. The electrical and structural characteristics of graphene models doped with Pb, U, and Pu analyzed using Density Functional Theory (DFT). The study focused on the double lead doped forms of graphene, where two lead (Pb) atoms placed on the same side in the Cis model and on opposing sides in the Trans model. The optimized models achieve structures with minimized energy, which validated by the calculated non-imaginary frequencies. Molecular and atomic characteristics analyzed to assess the impact of lead dopant on the structural and electronic properties of graphene in order to compare different models. This study get three models of Uranium-doped graphene, named (UG1), (UG2), and (UG3), based on the size of their surface layers, were analyzed, and the stable structures were determined. The electronic molecular orbital characteristics of these structures assessed as appropriate. The results demonstrated

that stabilized structures can be produce where the electrical characteristics vary based on size. The (UG3) model anticipated to have a higher degree of conductivity compared to the (UG1) model, which had a lower level. The energy levels of the HOMO and LUMO were proof of the electronic conductivity qualities' success. Ultimately, the dimensions of the (UG) model can influence its electronic characteristics for particular uses.

Plutonium (Pu)-doped conical Nano-carbon materials, (PuNC120), (PuNC180), and (PuNC240), created with separation angles of 120, 180, and 240 degrees, respectively, with the Pu atom doped at the apex of the conical structure. The results showed that the (PuNC120) model with four Plutonium-Carbon bonds had exceptional electrical and conductivity characteristics in this study. The model systems identified for additional applications based on their structural and electrical characteristics.

This work's primary accomplishments included effectively optimizing the models by enhancing the relevant information compared to other models. Future applications for these model systems could be anticipate based on the analyzed electronic characteristics.

Key Words : Graphene; Coronene; Density functional theory; Lead; Uranium, Plutonium; Conical Nano-carbons

Science Code : 20203

ÖZET

Doktora Tezi

AĞIR METAL KATKILI GRAFENİN MOLEKÜLER ÖZELLİKLERİNİN VE PİRENDEN OLUŞUMUNUN YOĞUNLUK FONKSİYONEL TEORİSİ İLE İNCELENMESİ

Lina Majeed Haider Al-HAIDERI

Karabük Üniversitesi
Lisansüstü Eğitim Enstitüsü
Fizik Anabilim Dalı

Tez Danışmanı
Prof. Dr. Necla ÇAKMAK
Ocak 2024, 65 sayfa

Bu çalışmada Coronene, moleküler ölçekte grafenin temsili bir yapısı olarak kabul edildi. Pb, U ve Pu katkılı grafen modellerinin elektronik ve yapısal özellikleri, yoğunluk fonksiyonel teorisi (DFT) yaklaşımı kullanılarak araştırıldı. Çift kurşun (Pb) katkılı grafen modelleri, Cis modelinde iki Pb atomunun grafenin aynı tarafına yerleştirilmesi ve Trans modelinde iki Pb atomunun karşıt taraflara yerleştirilmesiyle incelenmiştir. Modeller, değerlendirilen hayali olmayan frekanslarla doğrulanan minimum enerji yapılarını elde etmek için optimize edildi. İncelenen modeller arasında bir karşılaştırma yapmak amacıyla Pb katkı maddesinin grafenin yapısal ve elektronik özellikleri üzerindeki etkilerini tanımak için moleküler ve atomik özellikler elde edildi. Küçükten büyüğe (UG1), (UG2) ve (UG3) olarak tanımlanan farklı boyutlardaki yüzey katmanları ile U katkılı grafenin üç modeli ile incelendi ve stabilize yapılar elde edildi. Bu yapıların elektronik moleküler yörünge özellikleri buna göre değerlendirildi. Sonuçlar, elektronik özelliklerin boyuta bağlı olduğu stabilize yapıların gerçekten de elde edilebileceğini gösterdi. İletkenlik özelliğinin (UG3) modelinde daha yüksek düzeyde olması beklenirken (UG1) modelinde daha düşük

düzeyde olması bekleniyordu. En yüksek dolu ve en düşük boş moleküler yörüngelerin (HOMO ve LUMO) enerji seviyeleri, gerçekten de elektronik iletkenlik özelliklerinde böyle bir başarının kanıtıdır. Sonuç olarak UG' nin model boyutu, belirli uygulamalar için elektronik özelliklerini belirleyebilir.

Plütonyum (Pu) katkılı konik nano-karbon malzemelerin incelenmesi için Pu atomunun konik yapının tepesine katkıladığı 120, 180 ve 240 derecelik ayrım açılarıyla (PuNC120), (PuNC180) ve (PuNC240) modelleri elde edildi. Sonuçlar, dört Pu-C bağına sahip PuNC120' nin, dikkat çekici elektronik ve iletkenlik özellikleri gösteren bu çalışmanın seçkin modeli olduğunu gösterdi. Model sistemler, daha sonraki uygulamalar için belirlenecek yapısal ve elektronik özelliklere göre tanındı.

Bu çalışmanın ana kazanımları, modelin faydalı bilgilerinin diğer modellere göre geliştirilerek modellerin başarılı bir şekilde optimizasyonuydu. Araştırılan elektronik özelliklere dayanarak, bu tür model sistemler için daha ileri uygulamaların geliştirilmesi beklenebilir.

Anahtar Kelimeler : Grafen; Coronene; Yoğunluk fonksiyonel teorisi; Kurşun; Uranyum; Plütonyum; Konik nano-karbonlar.

Bilim Kodu **:** 20203

ACKNOWLEDGMENT

First and foremost, my great thank to my PhD supervisor, Prof. Dr. Necla ÇAKMAK for her high interest, help and guidance in the preparation of this thesis.

My thanks and gratitude to my PhD thesis committee members: Prof. Dr. TURHAN, Prof. Dr. HANÇERLIOĞULLARI, Prof. Dr. BALDIK, Assoc. Prof. Dr. ERER. Thank you for providing valuable feedback and thought-provoking questions. Your insights have greatly enriched the quality of my work.

I would also like to express my thanks and gratitude to whom encourage and support me in my work my parent.

Especial thank to my dear husband Prof. Dr. AAL-SHABEEB. I am profoundly grateful for the immeasurable contributions to both my academic and personal development. . My thanks and appreciation to my brother, sisters and children for the moral support. My thanks to Karabük University and all those who contributed and developed it.

CONTENTS

Page

Page

LIST OF FIGURES

Page

LIST OF TABLES

Page

SYMBOLS AND ABBREVIATIONS INDEX

SYMBOLS

B3LYP : Exchange-Correlation Functional

6-31G (d) : Basis Set

Cis : Conformation implied for doping double lead atoms at one side of graphene

Trans : Conformation implied for doping double lead atoms at the opposite sides of coronene layer

$\nabla^2 \rho$: Laplacian of charge density

ABBREVIATIONS

DFT : Density Function Theory

HOMO : Highest Occupied Molecule Orbital

LUMO : Lowest Unoccupied Molecule Orbital

EG : Energy Gap

NC : Nano Carbon

CH : Chemical hardness

Cs : Chemical softness

ESP : Electro Static Potential

QTAIM : Quantum Theory of Atoms in Molecules

QCC : Quadrupole Coupling Constant

FE : Fermi Energy

DM : Dipole Moment

IR : Infrared

CPU : Central Processing Unit

AOs : Atomic Orbitals

LCAO : Linear Combination of Atomic Orbitals

MOs : Molecular Orbitals

DOS : Density of States

ECP : Effective Core Potential

PART 1

INTRODUCTION

Since the inception of Nanotechnology, researchers have consistently endeavored to further the capabilities of this emerging technology and its associated nanostructures for a wide array of applications, including but not limited to air pollution mitigation and alterations of biological systems [1]. In addition to the inherent structure, presence of impurities has been seen to play a significant role in development of Nanostructures for various purposes [2]. The nanostructures may effectively capture exogenous chemicals under certain circumstances using atomically doped or molecule-functionalized models [3]. The study of nanostructures is important considering their distinctive capacity to capture or adsorb various substances [4]. The carbon nanotube (CNT) has been formally unveiled as the inaugural nanostructure within the realm of scientific and technological advancements [5].

Nevertheless, the aforementioned nanostructure is not the only nanostructure under consideration. Various alternative Nanostructures, exhibiting distinct forms and compositions, have been proposed and investigated via computer simulations and practical analyses [6]. Graphene, a single layer of carbon atoms, has also been presented as an additional Nano-structure, supported by experimental data [7]. The use of graphene's surface for the adsorption of various substances has been well recognized. This includes the production of doping and functionalized models, which can be achieve in this scenario [8, 9, 10]. Under oxidative circumstances, vacancies manifest on graphene surfaces, therefore creating favorable locations for the adsorption of additional atoms, including dopants [11]. The presence of metal element dopants on graphene surfaces has been observed as a potential avenue for pollution removal, highlighting the significance of this process [12–14]. Graphene monolayers have shown use in a diverse range of applications, including their potential usage as cathodes in electrochemical systems [15–17]. Furthermore, the use of Nano-carbon

structures as sensors is a common application whereby these structures possess the ability to both detect and remove chemicals that are being felt [18–20]. One of the primary challenges faced by high-tech enterprises pertains to the generation of waste materials, including lead (Pb). The proper disposal and elimination of these waste elements are crucial to safeguarding the environment from further contamination [21, 22]. Previous studies have shown the significance of graphene layers in the adsorption of heavy metal contaminants. However, it is important to note that this concept is still in the process of further development [12, 23, 24]. Hence, this study focuses on the examination of lead-doped graphene structures using Density Functional Theory (DFT) computations. Graphene, a single layer of carbon atoms, may be effectively studied at the molecular scale using coronene as a representative Nano flake [25–27]. Coronene ($C_{24}H_{12}$) given in Figure 1 has identified as a promising molecular surface for the adsorption of various atomic and molecular species [28, 29].

Following the groundbreaking advancements in Carbon Nanotube (CNT) technology, significant endeavors have been undertaken to investigate other nanostructures using computational modeling and experimental methods [30-32]. In this context, graphene, which refers to single-layered structures composed of carbon atoms arranged in a hollow-like configuration, has been shown to exist [33-35]. The suitability of graphene's surface as a catalyzed substrate for chemical processes, also its well-known electronic properties in the electronics field, has been observed. In this context, it has been shown that graphene, which consists of single-layered carbon atoms arranged in a hollow-like structure, is readily accessible [36-38]. The use of graphene surfaces has shown the potential for achieving the adsorption of many compounds, ranging from contaminants in industrial contexts to medicine delivery in living systems [39-41].

The presence of dopants is considered crucial for the emergence of distinctive electrical properties in nanostructures, alongside their inherent composition, in order to fulfill specific application requirements [42-44]. A comprehensive investigation has been conducted on atoms ranging from low weight to heavy atoms for the purpose of doping the surface of carbon like graphene. It is important to note that area of research is currently in the developmental stage [45-47]. The semiconductor function of atomically doped graphene systems has significant relevance since the presence of

dopants introduces novel characteristics to this function when compared to the pure carbon model [48-50]. To achieve this objective, the use of a computational method may provide valuable insights into the modeling of systems, particularly about the deterministic influence of doped atoms [51-53].

The first breakthrough in nanotechnology has catalyzed further investigations into many facets of this emerging field and its associated materials [54-56]. The two primary Nano-based materials that were first developed had tubular and spherical structural shapes. These materials were composed of carbon atoms and were therefore referred to as Nano-carbons [57-59]. Subsequently, a variety of other structural configurations of the Nano-carbons, including conical shapes, were devised to broaden the scope of nanomaterials [60-62]. In addition to the inherent carbon content of these nanostructures, the presence of atomic impurities, namely atomic dopants, has been seen as advantageous in the development of novel materials for usage in electrical systems [63-65]. The presence of atomic impurities may have a substantial impact on the electronic conductivity of Nano carbons, rendering them more appropriate for certain applications of semi-conducting [66-68]. In this context, acquiring knowledge about the characteristics of atomic-doped Nano carbons has the potential to facilitate advancements in the development of novel applications within the realm of electrical fields [69-71]. In order to achieve this objective, the use of molecular computations has the potential to unveil valuable insights into the molecular and atomic systems of Nano carbons at a small-scale level [72-74]. Based on previous studies, the use of atomic-doped conical Nano carbons has been recognized as significant in the context of exploring specific materials that engage in interactions with other materials and exhibit properties of semiconductor materials [75-77]. The introduction of a doped atom has the potential to modulate the performance of a Nano carbon material to cater to a particular application [78-80].

In this study, as shown in Section 1, the adsorption of the lead atom onto coronene was examined via the creation of mono and dual-doped models. Previous studies mostly focused on investigating graphene models doped with a single element, whereas the present study explores the concept of dual doping in graphene. To achieve this objective, an investigation was conducted on the Cis and Trans models of double-

doped coronene. The purpose was to examine impact of different locations of geometry on the stability of lead-doped models. The use of computer-based methods in this study has allowed for the examination of many characteristics of subjects at the atomic and molecular levels. This advantage has been effectively exploited in the present work to achieve the intended objective [81–83]. In addition, the development of new adsorbents, particularly those designed to target heavy metal pollutants, has consistently been a significant area of focus within the realm of environmental concerns. This research aims to safeguard human health in cities where industries generate substantial quantities of heavy metal waste [84]. The removal of contaminants, particularly heavy metals, has significant importance concerning the waste disposal practices of chemical, petrochemical, and nuclear sectors [85].

The second half of the present research study focuses on examining a model of graphene doped with uranium (U) atoms. The objective is to demonstrate the advantages of including uranium as an atomic dopant to generate new electrical properties in the graphene material under investigation. In order to accomplish this objective, a single uranium (U) atom was strategically replaced at the central position inside the graphene layer, resulting in the formation of bundled models doped with uranium (UG). In order to examine the impact of monolayer size in our study, we investigated three models that varied in terms of increasing surface diameter. In this context, quantum computations conducted to improve the geometries of the models and assess the associated descriptors that characterize the nature of the researched model systems. The primary goal of this investigation was to scrutinize the electrical and structural attributes of a graphene model subjected to uranium doping, with the intent of discerning the influence of atomic dopants on the unique characteristics inherent in the models under examination.

The present study focused on examining specific characteristics in the context of Part three. This was accomplished by conducting molecular computations on plutonium-doped models of conical Nano-carbon materials.

The results of this thesis study were published in one Q3 and two Q4-level scientific papers. It was also shared with the scientific community through oral presentations at two international conferences.

This thesis divided into seven broad sections. Introduction, the literature review, the theoretical background, and the methodology are given in Parts 1, 2, 3, and 4, respectively. The results and discussion, conclusions and summary are presented in Parts 5, 6, and 7, respectively.

PART 2

LITERATURE REVIEW

There have been and still and renewed many studies on the use of DFT to test various materials in various sciences such as physics, chemistry, and biology, and in various fields, including environmental, medical, biological, and applied. The most important studies related to this work selected as follows:

Ariaei et al. (2021) performed Density Functional Theory calculations to achieve selective adsorption surface of carbon monoxide (CO) and nitrogen monoxide (NO) molecules in a Nano-structure of $C_{16}Mg_8O_8$ to evaluate molecular properties, including energy levels HOMO, LUMO and energy gaps to obtain structures that can capture these gaseous to reducing environmental health problems related to them [86].

Dehaghani et al. (2020) analyzed the mechanical behavior of the original and defective Beryllium Oxide (BeO) Graphene-Like Nano Structures subjected to some shape defects (BeOGLNSs) structures and calculated Young's modulus and failure stress for circular and square cracks using simulations in molecular mechanics. The work concluded that the defects spread in a perpendicular direction to the stress load, and the increase in the dimensions of defect cause decreasing in the thermal negative effect on the failure stress [87].

In 2020, Rostamiyan et al. studied mechanical and electronic properties of the structures of single, double and triple-walled beryllium oxide Nano-tubes along with BeO Nano-peapods by using DFT. The simulations showed that increasing the radius and the distance between the walls led to a decrease in the Young's modulus for the single and double wall pipes, while the triple wall pipes did not show that difference. This increase led to an increase in the energy gap and a decrease in the formation energy. However, the Nano-peapods showed weaker mechanical and semiconductor

properties than the single-walled structure, and that the larger structure is more stable than the smaller one [88].

Khodashenas et al. conducted 2019 an experimental and theoretical study of the electronic structure of gold Nano-particles and then covered with gelatin as carriers for curcumin drugs, choosing the appropriate size for drug delivery through spectral and microscopic measurements, and verifying this using the DFT theory. The study revealed that the largest encapsulation is at 100 nm, and that the amount of curcumin drug that is released at pH= 7.4 is less than pH=5.4 [89].

In another study by Ghazali et al. in 2022 on the electronic and adsorption properties of the gold group (clusters) interacting with five- fluorine molecules in the gas phase using the Density Functional Theory (DFT) calculation. The simulation calculations in Monte Carlo in an aqueous solution showed that the individual clusters act appropriately as a carrier of fluorine, which means that it is more suitable for conducting Nano-medications for cancer [90].

The different adsorption sites of BN-doped Graphdiyne (BNGDY) Nano-sheet and pristine Graphdiyne (GDY) examined using DFT by Tabandeh et al. in 2021 and in the gas and solution phases of two types of anticancer drugs Hydroxyurea (HU) and 5-Fluorouracil (FU). The PDOS diagrams showed that the recovery time values in the domain of HU and FU drug delivery fit the structures of GDY and PNGDY, respectively [91].

Derdare et al. (2021) found using DFT with the B3LYB function about the adsorption of NO_2 NO_3 and NH_3 molecules on the surface of C_2O or MC_{19} (M = Ru, Ir and Au) groups, that NO_2 and NH_3 molecules can adsorb physically on the surface of C_2O, while N_2O is adsorbed chemically strongly, with an adsorption energy – 45.4 kcal/ mol. The interaction of these molecules with the group IrC_{19}, ArC_{19}, and RuC_{19} was also studied, where a large variation was observed in the energy gaps E_g of the AuC_{19} group, which leads to an increase in electronic conductivity. Therefore, this group has electronic sensitivity towards these molecules, which leads to an increase in electrical

conductivity as well. The effect of the solution on the electronic and adsorption properties was also studied [92].

In another study by the same researchers in 2022, DFT calculations and the theoretical B3LYP-D3/631G (d, p) level of theory were used with the MBOFMO or Frontier Molecular Orbital technique by Younes et al. in 2019. The change in the electronic structure of metallofullerene was observed by removing mustard gas, so it was considered an alternate fluorine C_2O tonic with Ni-Ti, and Fe. The results indicated that fluorine was an ideal candidate for the adsorption of mustard gas, with an adsorption energy that ranged between -96 and -102 kJ/mole [93].

Shyma et al. (2022), obtained significant changes in the optical properties and chemical specifications, and that the energy gap values decreased for all Nano-cluster systems when examining the adsorption of Sorbic acid drug on the surface of Coronene/Fullerene/ Fullerene like Nano-cages. Where an improvement in the wavenumber of the functional group in the Raman spectrum appeared, and thus it became possible to make a Nano sensor to detect these compounds, and it gave good values for atomic contact energies for drug delivery [94].

A similar study by Padash et al. in 2020 examined the adsorption of sulfa amide drug on the surface of Nanoparticles $Al_{12}N_{12}$, $Al_{12}P_{12}$, $B_{12}N_{12}$, and $B_{12}P_{12}$ using DFT and the theory of (QTAIM). Upon adsorption, the energy levels changed HOMO and LUMO significantly decreased energy beam, which enhances the electrical conductivity, and this is what makes them electronic sensors in addition to the possibility of delivering the sulfa amide drug in the biological system [95].

Derakhshandeh studied in 2021 was about conducting density functional theory DFT calculations about the adsorption of Boron trichloride on pristine graphene. The results confirmed that the interaction of BCl_3 with graphene is weak and therefore it is not possible to use this sheet as a sensor. It was also found that replacing the carbon atom of graphene with metal Cr reduces the HOMO-LUMO energy gap, in the doped graphene after adsorption of Boron trichloride BCl_3, which increases the electrical

conductivity and converts it into an electrical signal. Thus, Boron trichloride BCl_3 can be sensed by this process [96].

In 2021, Abbasi and Nemati-Kande conducted theoretical work to synthesize and test carbon nanotube (CNT) doped by boron (type-p) and nitrogen (n-type), to use them as carbon dioxide sensors as well as carbon monoxide detectors and removers using DFT and B3LYP-D3)/6-31+G (d, p) functional/basis set. Essentially, within the group of industrial applications and the detection of environmental pollutants, where this group of nanoparticles dotted with different concentrations of boron and nitrogen showed unexpected chemical and physical reactions, then the appropriate ones were chosen to achieve the highest efficiency [97].

Wang et al. (2022) studied theoretically the effect of chemical doping concentration with metals (Ni, Pd, Pt) on the adsorption potential of monolayer $MoTe_2$ to absorbed (CO). Using DFT to calculate the optimal geometry, band structure (BC), adsorption parameters, and the density of states for adsorption of CO or on the $MoTe_2$ and TM-$MoTe_2$ surfaces. The results indicated that the adsorption of monolayer $TMoTe_2$ is stronger than the effect of internal $MoTe_2$ [98].

PART 3

THEORETICAL BACKGROUND

Quantum computations were executed to refine model geometries and assess descriptors crucial for characterizing the studied model systems. It is essential to underscore that the primary focus of this research revolved around investigating the electronic and structural attributes of graphene models doped with Pb, U, and Pu. The overarching goal was to discern the effects of atomic dopants on the emergence of unique features within the scrutinized models.

3.1. DENSITY FUNCTIONAL THEORY (DFT)

Within this segment, we will delve into pivotal theories and approximations formulated by scientists to analyze physical systems that posed challenges for conventional quantum mechanics. Foremost among these approximations stand the Born-Oppenheimer and Hartree-Fock approximations. Additionally, a comprehensive exploration of Density Functional Theory (DFT) will ensue, underscoring its fundamental role in simplifying the Schrödinger equation by treating energy as a functional of the total electron density.

3.2. THE SCHRÖDINGER EQUATION FOR CRYSTAL

The Schrödinger equation serves as the fundamental cornerstone for conducting comprehensive quantitative analyses of the inherent quantum properties within material system [99].The resolution of the time-independent Schrödinger equation facilitates the attainment of a detailed representation of any microscopic system. This achievement is contingent upon a nuanced comprehension of the dynamics manifested by its elemental constituents, specifically electrons and nuclei [100]. The time-independent Schrödinger equation is in the following form:

$$H\psi = E\psi \tag{3.1}$$

Where H, E and ψ are the Hamilton system, the total energy of the system, and the wave function of the system, respectively.

The Hamiltonian of a crystal system encompasses numerous particles engaged in mutual interactions. It is composed of the aggregate kinetic energy of all particles and the potential energy arising from interactions among them. In the absence of external field interactions, the Hamiltonian is expressed as follows:

$$H = T_e + T_n + V_{e\text{-}e} + V_{e\text{-}n} + V_{n\text{-}n} \tag{3.2}$$

$$T_e = -\hbar^2/2M_e \sum_{i=1}^{Ne} \nabla_i^2 \tag{3.3}$$

$$T_n = -\hbar^2/2M_n \sum_{i=1}^{Nn} \nabla_i^2 \tag{3.4}$$

$$V_{e\text{-}e} = \sum_{i,i\neq j} \frac{1}{4\pi\varepsilon o} \frac{1}{2} \left(\frac{e^2}{|ri - rj|} \right) \tag{3.5}$$

$$V_{n-n} = \sum_{\alpha\neq\beta} \frac{1}{4\pi\varepsilon_o} \frac{1}{2} \left(\frac{z_\alpha z_\beta e^2}{|R_\alpha - R_\beta|} \right) \tag{3.6}$$

$$v_{n-e} = \sum_{i,\alpha} \left(-\frac{1}{4\pi\varepsilon_0} \right) \left(\frac{z_\alpha e^2}{|r_i - R_\alpha|} \right) \tag{3.7}$$

Where T_e: the kinetic energy of electrons, T_n: the kinetic energy of the nuclei, $V_{e\text{-}e}$: electron-electron interaction energy (repulsion energy), $V_{e\text{-}n}$: electron-nuclear interaction energy (attractive energy), $V_{n\text{-}n}$: nucleus-nuclear interaction energy (repulsion energy), i and j are coefficients for electrons, α and β: nuclei-specific coefficients. Also, M_e and M_n: the masses of electrons and nuclei, z_α and z_β: the atomic numbers of the nuclei α and β, $\left|r_{i-r_j}\right|$: the distance between the two electrons i and j. $\left|R_\alpha - R_\beta\right|$: The distance between the nuclei α and β, $|r_i - R_\alpha|$: the distance between the electron i and the nucleus α, and z_α e : the charge of the nucleus.

The Laplace parameter is given by

$$\nabla^2 = \frac{\partial}{\partial x^2} + \frac{\partial}{\partial Y^2} + \frac{\partial}{\partial Z^2} \quad (3.8)$$

The energy and wave functions of the system can be found by solving the Schrödinger equation:

$$(T_e + T_n + V_{e-e} + V_{e-n} + V_{n-n})\psi(R_1, R_2, \dots r_1, r_2) = E\psi(R_1, R_2, \dots., r_1, r_2) \quad (3.9)$$

Solutions to this time-independent equation can be found precisely in the case of hydrogen systems only, while in the case of a multi-electron system, and due to the many electronic interactions between the constituent particles of the system, there is no exact solution.

For the Schrödinger equation [101] example, but not limited to the Schrödinger equation for N atom containing 3 (Z +1) N variables, for example, when Z = 14 in 1 cm^3, we have approximately $2x10^{24}$ unknowns. That is, the Schrödinger equation in this way is impossible to solve, so several approximations have been made to simplify this equation. We will touch on some of them [99].

3.2.1. Born-Oppenheimer Approximation

Termed the adiabatic approximation, this method relies on segregating the motion of electrons from that of nuclei, exploiting the substantial contrast in both speed and mass between these entities. Specifically, the mass ratio (m_p=1836 m_e) underscores the considerable mass differential, with nuclei possessing significantly greater mass than electrons. Simultaneously, the considerable swiftness of electrons compared to nuclei underscores the significant speed distinction. The equations governing this approximation are solved under the assumption of static nuclei, disregarding their kinetic energy. [101].

The Hamiltonian divided into two parts the electronic part and the nuclear part

$$H_{elec.} = T_e + V_{n-e} + V_{e-e} \quad (3.10)$$

$$H_{nuc.} = T_n + V_{n-n} \approx V_{n-n} \tag{3.11}$$

So, the Schrödinger equation becomes

$$(T_e + V_{e-e} + V_{e-n} + V_{n-n})\,\psi(R_1, R_2, \ldots r_1, r_2) = E\psi(R_1, R_2, \ldots\ldots, r_1, r_2) \tag{3.12}$$

This approximation is very easy to solve the equation, however, due to the dependent movement of electrons and their strong electron-electron interactions, another approximation is needed.

3.2.2. Hartree Approximation

Referred to as the mean-field approximation, the Hartree approximation relies on an electron-independent model wherein each electron moves autonomously within an average field generated by the nuclei and other electrons. Consequently, the problem transitions from one involving numerous electrons to that concerning a single electron [102-104]. This paradigm shift facilitates the description of the electronic system's wave function as a direct product of individual electronic functions. [105] so that:

$$k(r_1, r_2, \ldots\ldots\ldots) = \prod_{i=1}^{Ne} \psi_i(r_i) = \psi_1(r_1)\psi_2(r_2) \ldots\ldots\ldots\ldots \psi_{Ne}(r_{Ne}) \tag{3.13}$$

The energy of the system becomes the sum of the energies of all the electrons:

$$E_e = \sum_{j=1}^{N_e} E_i \tag{3.14}$$

The Hamiltonian for the electron *i* can be written as:

$$H_i = \frac{-\hbar^2}{2m}\nabla_i^2 + U_i(r_i) + V_i(r_i) \tag{3.15}$$

Where $V_i(r_i)$ is the effective potential for Hartree-Fock, and given by

$$V_i(r_i) = \frac{1}{2}\sum_{i,i\neq j}\left(\frac{K_e^2}{|r_i - R_j|}\right) \tag{3.16}$$

$$U_i(r_j) = -\sum_\alpha \frac{z_\alpha \alpha e^2}{|r_i - R_\alpha|} \tag{3.17}$$

The potential energy of the electron i in the nucleus field. So we can write the one-electron Schrödinger equation which is called the Hartree equation as follows:

$$\left(\frac{-\hbar^2}{2m}\nabla_i^2 + U_1(r_i) + V_i(r_i)\right)\psi_i(r_i) = E\psi_i(r_i) \tag{3.18}$$

3.2.3. Hartree Fock Approximation

In 1932 AD, the scientist Focke showed that the Hartree wave function (Schrödinger equation for one particle) does not satisfy the Pauli Exclusion Principle [36]. Due to the fermionic nature of electrons, the wave function exhibits symmetry upon the exchange of any two electrons. Hartree, however, overlooked this characteristic, prompting Fock to rectify the deficiency by incorporating the spin principle into the electron system. This augmentation ensures compliance with the Pauli Exclusion Principle, thereby introducing an N! Probability factor for the arrangement of N electrons in distinct positions. [105-107]:

For example, the first possibility of placing N electron in position N is written as:

$$\psi_1(r_1)\psi_2(r_2)\psi_3(r_3) \dots\dots\dots\dots\psi_N(r_N) \tag{3.19}$$

Another possibility is given by:

$$\psi_1(r_1)\psi_2(r_3)\psi_3(r_2) \dots\dots\dots\dots\psi_N(r_N) \tag{3.20}$$

Thus, applying all the substitutions, we get the N! Limit of the same type. The wave function is the sum of all the terms, taking into account the (+) and (-) signs so that each determinant is called a Slater determinant [106] and given by:

$$\psi_e = \psi_e(r_1, r_2, r_3 \dots \dots, r_n) = \frac{1}{\sqrt{N!}}\begin{vmatrix} \psi_1(r_1)\psi_1(r_2)\ldots\ldots\ldots\psi_n(r_n) \\ \psi_n(r_1)\psi_n(r_2)\ldots\ldots\ldots\psi_n(r_n) \end{vmatrix} \quad (3.21)$$

Where: $1/\sqrt{N!}$ is a constant monotheism. The new Hartree-Fock equation for a single particle system becomes as follows.

$$E = \int \psi^*(r_1, r_2, r_3, ..)\left[\left(\frac{-\hbar^2}{2m}\nabla_i^2 + U_i(r_i, \dots . R_1 \dots \dots)\right)\right]\Psi(r_1, r_2, r_3 \dots ..)dr +$$

$$\frac{1}{2}\sum_{i=j}\int \psi^*(r_1, r_2, r_3 \dots \dots)\frac{e^2}{r_{ij}}\psi(r_1, r_2, r_3 \dots .)dr \quad (3.22)$$

It can also be written as follows

$$-\frac{\hbar^2}{2m}\nabla_i^2\psi_i(r) + V_i(r)\psi_i(r) + V_H(r)\psi_i(r)\sum_j\int\frac{dr}{|r-r'|}\psi_j^*(r')\psi_i(r')\psi_j(r) = E_i\psi_i(r) \quad (3.23)$$

The differentiating factor distinguishing the Hartree approximation from the Hartree-Fock approximation lies in the inclusion of the exchange potential term, delineated as:

$$V_X = -\sum_j\int\frac{dr}{|r-r'|}\psi_j^*(r')\psi_i(r')\psi_j(v) = E_i\psi_i(r) \quad (3.24)$$

Using this approximation the computation becomes somewhat cumbersome and, in addition, imprecise the Hartree-Fock approximation neglects an important quantum interaction, which is the energy of the correlations between electrons with opposite spins. Among the difficulties encountered in calculating the structure of the energy bands is to determine the potential inside the crystal, where the probability of the presence of an electron in position r depends on the presence of electrons in position r'. As a result, the energy obtained by the Hartree-Fock (E_{HF}) approximation is always exaggerated.

A very effective and promising alternative to overcome these difficulties is a practical method known as the density functional theory [108].

3.2.4. Density Functional Theory

In contrast to antecedent methodologies reliant upon the utilization of multiple electron wave functions, Density Functional Theory (DFT) constitutes a reconfiguration of the quantum N-particle predicament, effectively recasting it as a tow-particle quandary or, more precisely, a bipartite challenge when incorporating the considerations of "up" or "down" spin. Through the substitution of functions, DFT employs the electronic density as a foundational variable in its calculations. In this paradigm, the energy of an electronic system is articulated in terms of its density, wherein the count of electrons in the system (N_e) is supplanted by the total electron density ρ(r), a function contingent upon spatial coordinates (x, y, z). [102, 109], and the energy of the system can be written in the form:

$$E = E(\rho) \tag{3.25}$$

The inception of Density Functional Theory (DFT) traces back to the endeavors of Thomas and Fermi in the latter part of the 1920s. Subsequently, in the mid-1960s, Hohenberg-Kohn and Sham laid the groundwork for the theoretical framework upon which the contemporary method is founded [108,110-112].

3.2.4.1. Thomas-Fermi Theorem

In the year 1927 AD, Thomas and Fermi formulated the total energy of a gas of heterogeneous electrons as a function of the known electron density for a homogeneous gas [110, 111]. By making several divisions on the Brillouin region, which is a local approximation that does not take into account the electrons correlation, that is, it is a statistical model for approximating the electronic distribution around atoms. Since at the last division, the electronic density is considered constant in each of the divided regions of Brillouin [110, 111, 113]. This model gave a picture of the possibility of relying on the electronic density to calculate the kinetic energy, and the total energy of the system (E) in the following form:

$$E = \int \varepsilon_i[\rho(r)]\, dr \tag{3.26}$$

The density of a homogeneous gas is given by:

$$\rho = E_f^{\frac{3}{2}} \left(\frac{2m_e}{h^2}\right) \frac{1}{3\Pi^2} \tag{3.27}$$

The kinetic energy of a homogeneous gas is given by:

$$T = \frac{3}{5}\rho E_f \tag{3.28}$$

Where ε_i is the energy of the system at position x, ρ is the density of the homogeneous gas, and E_f is the Fermi energy.

From the previous two equations 24 and 25 we find by:

$$E_f = \frac{h^2 \rho^{\frac{2}{3}}}{2m_e} (3\pi^2)^{\frac{2}{3}} \tag{3.29}$$

$$T = \frac{3}{5} \frac{h^2 \rho^{\frac{5}{3}}}{2m_e} (3\pi^2)^{\frac{2}{3}} \tag{3.30}$$

The kinetic energy of Thomas-Fermi is given as:

$$T_{TF} = \int T\, dr \tag{3.31}$$

And

$$T_{HF} = \frac{3}{5} \frac{h^2}{2m_e} (3\pi^2)^{\frac{2}{3}} \int \rho^{\frac{5}{3}}\, dr \tag{3.32}$$

As previously indicated, the Thomas-Fermi theorem constitutes a localized approximation of electron density, devoid of considerations for electron bonding.

Consequently, the total energy expression for the system of electrons within the ambit of the Thomas-Fermi approximation is articulated as follows:

$$E_{TF} = \frac{3}{5}\frac{h^2}{2m_e}(3\pi^2)^{\frac{2}{3}}\int \rho^{\frac{5}{3}}\,dr + \int V(r)\rho(r)\,dr + \frac{1}{2}\int \frac{\rho(r)P(r')}{|r-r'|}\,drdr' \quad (3.33)$$

Also, some improvements made to this theory. Firstly, the exchange effect proposed by Dirac

$$E_{TFD} = E_{TF} - C_x\int \rho^{\frac{4}{3}}\,dr \quad (3.34)$$

Secondly, the linking effect suggested by Fegins [102]

$$E_C[\rho] = -\frac{0.056\rho^{\frac{4}{3}}}{0.079+\rho^{\frac{1}{3}}} \quad (3.35)$$

3.2.4.2. Hohenberg and Kohn's Theories

In the year 1964 AD, the two scientists Hohenberg and Kohn set the basic rule for the functional theory of density through their theory, which proved the possibility of exploiting density in calculating the properties of the system, but it remained without application until the scientist completed what he started with and found an application for it. The Hohenberg-Kohn theory applies to any system of interacting particles and is summarized in two basic theories:

First theory for any particle system in the basic state in interaction with an external potential (V_{ext} potential of the nuclei), the total energy of the system is known as the electronic density (ρ), i.e. all the properties of the system can be known if the electronic density is known:

$$E = E_p \quad (3.36)$$

$$E(r) = F[\rho] + \int \rho(r)V_{ext}(r)\,dr \quad (3.37)$$

Where $\int \rho(r) V_{ext}(r)\, dr$ represent an electron-nucleus interaction. F[ρ] is the Hohenberg-Kohn function and it is defined as a single function for any poly electron system and can be written as follows:

$$F(\rho) = T[\rho(r)] + V_{e-e}[\rho(r)] \tag{3.38}$$

F[ρ] is a comprehensive function of the electron density. T [ρ (r)] is the kinetic energy of the electronic system. $V_{e\text{-}e}$ [ρ (r)] is the electron-electron interaction energy. However, the analytic expression for these two values is not known.

The second theory posits that the minimum aggregate energy of the system aligns with the electronegativity of the fundamental state $E_{\rho fund}$ (r), expressed as:

$$E_{\rho fund}(r) = \min E(\rho) \tag{3.39}$$

$$E(\rho) = \langle \psi | H | \psi \rangle \tag{3.40}$$

$$E(\rho) = \langle \psi | T + V | \psi \rangle \tag{3.41}$$

$$E(\rho) = \langle \psi | F(\rho) | \psi \rangle \tag{3.42}$$

Where, T is the kinetic energy of the electrons, V is the potential of the interaction of electrons, and F (ρ) is a comprehensive function of the electron density. So, by knowing F (ρ) we can calculate the electronic properties of all the systems.

3.2.4.3. Kohn-Sham equation

The motion of electrons is difficult to describe precisely in terms of their electron density, and the Pauli Exclusion Principle makes things even more complicated because of the different functions that must be considered [108]. By setting simulated equations to the Schrödinger equation to determine the wave functions that correspond to the lowest value for the total energy. So, this problem has been overcome by using an actual system of independent (non-interacting) electrons that are subject to effective

external potentials V_{eff} (r) resulting from the nuclei and other electrons, so that they have the same electronic density as the real system, taking into account the Pauli principle [40] and given energy Kohn-Sham with the following relationship:

$$E_{ks} = F(\rho) + \int \rho(r) V_{ext}(r) dr \tag{3.43}$$

$$E_{ks} = T_s(\rho) + E_H(\rho) + E_{XC}(\rho) \int \rho(r) V_{ext}(r) dr \tag{3.44}$$

$$T_S = \sum_{i=1}^{Ne} < \psi_i \left| \frac{-h^2}{2m} \nabla_i^2 \right| \psi_i > \tag{3.45}$$

$$E_H = \frac{e^2}{2} \int \frac{\rho(r)\rho(v')}{|r-r'|} d^3r \tag{3.46}$$

T_S is the kinetic energy of the independent electrons, it can be written based on the electronic states of a single particle, and E_H is the Hartree energy or coulomb interaction energy related to the self-interaction of electron density.

The description of the states of free electrons depends on both the Hartree energy and its kinetic energy. Mathematically, the difference between the real kinetic energy and the energy of unreacted electrons in addition to the difference between the real interaction energy and the Hartree energy is taken in the expression exchange-correlation energy [114] E_{xc}, which is given in the following:

$$E_{xc}(\rho) = [T(\rho) - T_s(\rho)] + [V_{ee}(\rho) - E_H(\rho)] \tag{3.47}$$

By applying the principle of covariance [23] is obtained as follows:

$$\frac{\delta E_{xs}}{\delta \Psi_i^*(r)} = \frac{\delta T_5}{\delta \psi_i^*(r)} + \left[\frac{\delta E_H}{\delta \rho(r)} + \frac{\delta E_{xc}}{\delta \rho(r)} + \frac{\delta E_{ext}}{\delta \rho(r)} \right] \frac{\delta \rho(r)}{\partial \psi_i^*(r)} \tag{3.48}$$

And, by applying the condition of maintaining the settlement written $\langle \Psi_i | \Psi_j \rangle = \delta_{ij}$. We get the so-called Kohn-Sham equations, and given as:

$$H_{KS}\Psi_i(r) = \left(T_s + V_{eff}(r)\right)\Psi_i(r) = \varepsilon_i\Psi_i(r) \quad (3.49)$$

$$\rho(r) = \sum_{i=1}|\Psi_i(r)|^2 \quad (3.50)$$

$$V_{eff} = V_H + V_{XC} + V_{ext} \quad (3.51)$$

$$V_{eff} = \frac{\delta E_H}{\delta\rho(r)} + \frac{\delta E_{XC}}{\delta\rho(r)} + \frac{\delta E_{ext}}{\delta\rho(r)} \quad (3.52)$$

Where $V_{XC} = \frac{\delta E_{XC}}{\delta\rho(r)}$ is the exchange-correlation potential.

3.3. KOHN-SHAM EQUATION SOLUTIONS

Most of the methods for calculating the structure of energy bands are based initially on the density functional theory, considering its use of density, in addition to Kohn-Sham orbits, and the basic wave function is given as follows [99,115]:

$$\Psi_i(r) = \Sigma c_{ij}\varphi_j(r) \quad (3.53)$$

Where C_{ij} is the propagation parameters of the wave function. φ_j is the wave function. The solution to the Kohn-Sham equation requires defining the coefficient C_{ij} for each occupied orbit, so that the total energy is at the minimum value. The total energy is calculated in highly symmetric points in the first Brillouin region to make the calculation easy, and due to the presence of repulsive forces between the electrons for their negative charge, an iterative loop was used and represented in the figure below, and for approximation required the initial density of the charge ρ_{in} in the calculation. The solutions to the Kohn-Sham equation given by the following relationship:

$$(H - \varepsilon_i S)C_i = S \quad (3.54)$$

Where H: the Hamilton Kohn-Sham, and S is the coverage matrix.

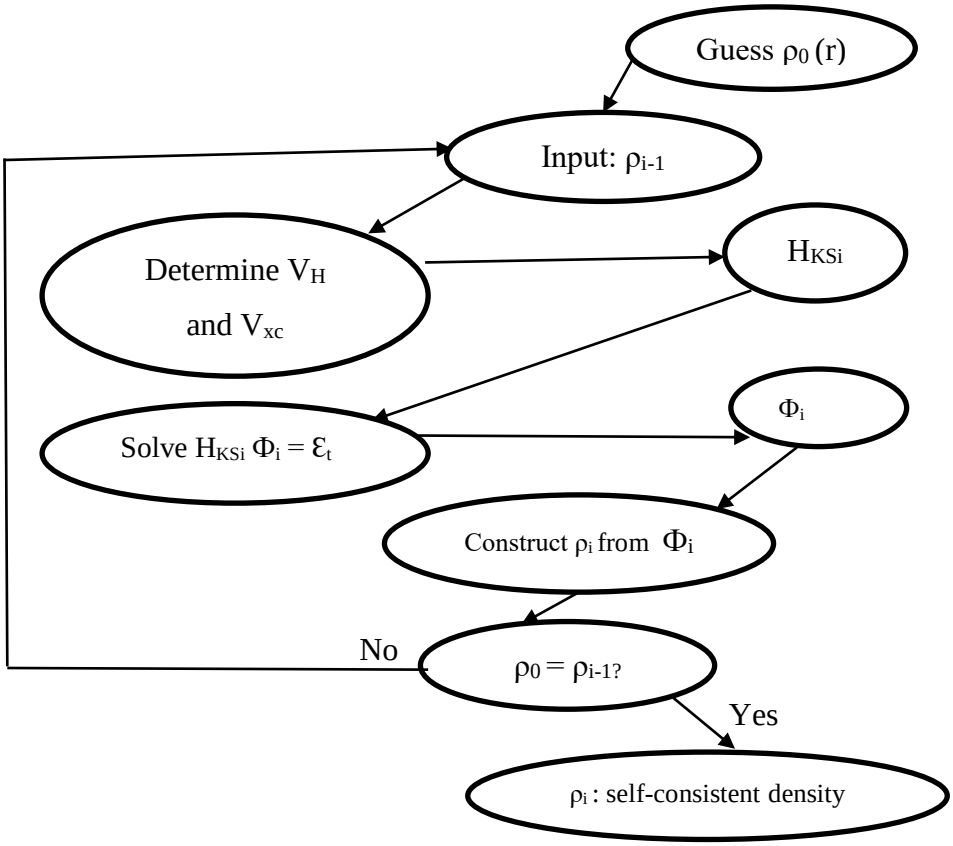

Figure 3.1. Kohn-Sham equation solution algorithm.

3.4. EXCHANGE CORRELATION FUNCTIONS

The results given by the density functional theory depend mainly on how accurately the exchange-correlation potential described. The main drawback of the Kohn-Sham method is the ambiguity of the term exchange-correlation potential, which makes solving the equations difficult [113].

$$\varepsilon_{XC} = \varepsilon_X + \varepsilon_C \tag{3.55}$$

Therefore, the exchange-correlation potential has gone through several approximate processes, so we cannot reach the accurate and exact form of this potential.

3.4.1. Local Density Approximation

This approximation was put forward by Kohn and Sham in 1965 A.D, represented by the local density approximation (LDA) to solve the problem of the exchange-

correlation function. The approximation of local density approximates the heterogeneous system of electrons as being locally or locally homogeneous, that is, it considers that most solids are close to the electron gas limits [99, 116].

The mean idea on which this approximation based, is that using the results of a homogeneous electron gas with a density equal to the local density of the heterogeneous system, by taking it on infinitesimal parts. Thus, we can determine the value of the exchange-correlation energy, and thus obtain a good description of the properties of the base state [113]. The exchange-correlation energy in this approximation given by the following relationship:

$$E_{xc}^{LDA}(\rho) = \int \rho(r)\varepsilon_{xc}(\rho(r))\, d^3r \tag{3.56}$$

Knowing that the exchange-correlation energy divided into two parts contributing to the link and contributing to the exchange:

$$\varepsilon_{xc}\left(\rho, r\right) = \varepsilon_x\left(\rho, r\right) + \varepsilon_c\left(\rho, r\right) \tag{3.57}$$

The exchange contribution determined by the Dirac equation for a homogeneous gas:

$$\varepsilon_c = -\frac{3}{4}\left(\frac{3}{\pi}\right)^{\frac{1}{3}} \rho(r)^{\frac{1}{3}} \tag{3.58}$$

As for the correlation contribution which is difficult to assess and is usually determined by quantum Monte Carlo simulations.

3.4.2. Generalized Gradient Approximation

The local density approximation (LDA) was taken on the electron gas model where the electronic density is homogeneous, while the atomic or molecular systems are very different from the homogeneous electron gas. In general, we can consider that all systems are heterogeneous, that is, the electronic density is not homogeneous and

varies from one position to another, this is what led to the emergence of the generalized gradient approximation (GGA) and it is also called the non-local approximation [99,117,118].

This approximation is a correction to the position density approximation as it exceeds it in accuracy and adds the electron density changes ρ across its gradient [117], and the energy expression written with the following relationship:

$$E_{xc}^{GGA}(\rho) = \int \varepsilon_{xc}([\rho], |\nabla\rho|) d^3r \tag{3.59}$$

3.4.3. Local Spin Density Approximation

The use of the electronic spin principle or the so-called Pauli principle gives an additional degree of freedom, so the two scientists Kohn and Sham used the LSDA approximation for magnetic systems by extending LDA to LSDA in order to determine the exchange-correlation energy. Where the exchange-correlation energy is a function of the up and down spin densities of two electrons have the same energy, which determines the density of the associated electrons in the case of spin up and down [119].

The expression exchange-correlation energy in this case is of the form:

$$E_{xc}^{LSDA}(\rho\uparrow, \rho\downarrow) = \int \rho(r)\, \varepsilon_{xc}\left(\rho\uparrow(r), \rho\downarrow(r)\right) d^3r \tag{3.60}$$

3.5. HYBRID FUNCTIONS

The third generation of functions is the so-called hybrid functions that depend on the form of adiabatic communication, in addition to the full or partial use of the Hartree-Fock (HF) exchange in the Kohn-Sham equation [120]. The adiabatic contact formula theoretically justifies the determination of the HF exchange energy from the energy of the Kohn-Sham orbits. In 1993 AD, the first job was proposed, which is the one proposed by Axcel Becke, and it contains 50% of the Hartree-Fock exchange energy, this function is also known as “half and half” [121]. There are several other hybrid

functions, the most important of which are LYP, MPWPW9, PW91, PW8 and the most widely used currently.

It is known by the acronym B3LYP [122]. The positional exchange functions, in addition to the Beck exchange and the Hartree-Fock exchange, in the correlation part they use the link-local (VWN) functions and gradient correction "Lee", "Yang" and "Parr:"

$$E_{XC}^{B3LYP} = E_{XC}^{LSDA} + a_0(E_{xc}^{HF} - \varepsilon_x^D) + a_X(E_X^{B88} - \varepsilon_x^D) + a_c(E_C^{LYP} - E_C^{VWN}) \qquad (3.61)$$

Where E_X^{B88} the correlation function for "Becke." E_C^{LYP} is the Correlation Function for "Lee", "Yang" and "Parr". E_C^{VWN} the Correlation Function of "Fusco" and colleagues. P W means Perdrew-Wang. The values of the parameters are also given a_0=0.2, a_X=0.72, and a_C=0.81, respectively. They are determined by optimizing the decay energies, ionization energy, electron or proton attractions of a group of test particles, and can also be considered as variables.

3.6. TIME-DEPENDENT DENSITY FUNCTIONAL THEORY

The time-dependent density functional theory (TD DFT) is a very necessary and important theory in order to study excited structures (excitation energy, polarization, and optical properties), and the time-dependent Kohn-Sham equations written in the following form [123]:

$$i\frac{\partial}{\partial T}\phi_i^{KS}(r_1,t) = H\phi_i^{KS}(r_1,t) = \left[\frac{-1}{2}\forall^2 + V_{eff}(\rho)(r_1,t)\right]\phi_i^{KS}(r_1,t) \qquad (3.62)$$

$$\rho(r_1,t) = \sum_{i=1}^{n}\left|\phi_i^{KS}(r_1,t)\right|^2 \qquad (3.63)$$

The effective potential in terms of time is given as follows:

$$V_{eff}(r_1,t) = V_{ext}(r_1,t) + \frac{1}{2}\iint \frac{\rho(r_1,t)\rho(r_2,t)}{r_{12}}dr_1\,dr_2 + V_{XC}(r_1,t) \qquad (3.64)$$

The density is determined, and its calculations developed based on Taylor series. We find that many properties such as polarization and excitation energy require only the first law of Taylor series, the latter depends on the function χ, which represents the linear response. After the Fourier transform, we can substitute the equation for time.

The equation related to frequency is as follows [52]:

$$\delta\rho(r_{1,\omega}) = \int x(r_1, r_{2,\omega})\delta V_{ext}(r_{2,\omega})\, dr_2 \tag{3.65}$$

Kohn and Sham write time-related equations by substituting the linear response function χ by the function χ_s of a non-interactive system, which we call the "non-interactive Kohn-Sham system", and the external potential replaced by the effective Kohn-Sham potential, where:

$$\chi_s(r_1, r_2, \omega) = \sum_{ij} \left(n_j - n_i\right) \frac{\phi_i(r_1)\phi_j^*(r_1)\phi_i(r_2)\phi_j^*(r_2)}{\omega - (\varepsilon_i - \varepsilon_j) + i\eta} \tag{3.66}$$

In the TD DFT, the electronic density of the non-interactive Kohn-Sham of the system given as:

$$\delta\rho = x_s \delta V_{eff} \tag{3.67}$$

The change in the effective potential δV_{eff} is written as the sum of three types of potential. $\int \frac{\delta\rho(r_1,\omega)\delta\rho(r_2,\omega)}{|r_1 - r_2|} dr_1\, dr_2$ Is the Coulomb potential, $\delta V_{ext}(r_1, \omega)$ is the external potential, and $\delta V_{xc}(r_1, \omega)$ is the Exchange-Correlation potential. The sum of potential is written by:

$$\delta V_{eff} = \int \frac{\delta\rho(r_1,\omega)\delta\rho(r_2,\omega)}{|r_1 - r_2|} dr_1\, dr_2 + \delta_{ext}(r_1, \omega) + \delta_{xc}(r_1 \cdot \omega) \tag{3.68}$$

3.7. LIMITATIONS AND PROSPECTS OF DENSITY FUNCTIONAL THEORY

Due to the density functional theory presented by many physical and chemical properties of materials, it has taken the interest of many scientists and physical and chemical research. It overcame many of the difficulties encountered by previous quantum theories. However, despite the advantages of this theory, it still contains many defects and problems.

The most important of these problems is the use of approximations in describing multiple systems. There are no precise rules or criteria for choosing a function without another. Despite these shortcomings, the density functional theory is still the basis and the best among the currently known approximations, and it is always in continuous development to overcome these shortcomings.

PART 4

METHODOLOGY

A theoretical model or approach involves representing a system by employing a designated set of approximations. These approximations, coupled with a computational algorithm, utilized on atomic-orbitals, as defined by the chosen basis set. The goal is to calculate molecular-orbitals and energy. Broadly categorized, these methods fall into four main types: semi-empirical, *ab*-initio, density functional, and molecular mechanics. The choice of a theoretical model relies on both the system's size and desired approximation level. (DFT) methods have gained increasing popularity due to their comparable results with ab initio methods, accompanied by a significant reduction in (CPU) time [124]. Differing from (HF) calculations, (DFT) utilizes electron density for energy computation instead of a wave function. The theoretical models based on DFT are recognized for providing optimal results in accordance with experimental values. [125]. All theoretical models require us to choose a basis set as start point for work.

A basis set comprises wave-functions that depict form of Atomic-Orbitals (AOs). In the chosen theoretical model, molecular-orbitals (MOs) are calculated by linearly combining these (AOs) through the Linear Combination of Atomic Orbitals (LCAO) method. For instance, PMn (n=3, 4, 5, 6) models employ an internal basis set, while ab initio or density functional theory necessitate a specified basis set. The level of approximation in our calculations is directly linked to the chosen basis set. The decision-making process involves striking a balance between result accuracy and CPU time. [124, 125].

This study included the use of (DFT) calculations to conduct molecular and atomic investigations, with the aim of exploring electronic and structural characteristics. The investigation was divided into three distinct components.

4.1. LEAD ATOM

We opted for a representative graphene model (Figure 5.2) to undergo doping with either one or two lead atoms, leading to the creation of mono and dual lead-doped models (Figure 5.3). In Figure 5.2, the atomic positions of the dopants are illustrated. The single-doped model features a single lead atom at one site, while the double-doped model includes lead atoms at both sites in both same sides (Cis) and opposite sides (Trans) conformations. The same sides conformation is recommended for doping double lead atoms on one side of the graphene structure, while the opposite sides conformation is suggested for doping double lead atoms on opposite sides of the coronene layer. Each model was individually optimized to attain lowest energy levels corresponding to optimized geometry. Subsequently, the optimized structures underwent additional frequency computations to ensure the absence of any imaginary frequencies. Consequently, three models selected post-optimization and frequency calculations, comprising single lead doped model and double lead-doped models in Cis (same sides) and Trans (opposite sides) conformations, as illustrated in Figure 5.3. The (B3LYP) Exchange-Correlation Functional, previously employed in a related study, utilized for the calculations. The Hydrogen and Carbon atoms described using the 6-311G (d, p) basis set, while the lead atom described using the LANL08d with Effective Core Potential (ECP) basis set within the Gaussian programmed [126, 127]. Furthermore, the optimized structures were assessed for their bond lengths and Infrared (IR) spectra, as seen in Figure 5.3. Table 5.1 presents a summary of the molecular properties derived for the optimized models, which include total Energies (E), Highest Occupied Molecular Orbitals (HOMO), Lowest Unoccupied Molecular Orbitals (LUMO), Energy-Gap (EG), Fermi-Energy (FE), Electric Dipole-Moment (DM), and Volume (V). Furthermore, Fig.5.3 illustrates the graphical representation of many electronic characteristics, including Electrostatic Potential (ESP) surfaces, energy level patterns of Highest Occupied Molecular Orbital (HOMO), Lowest Unoccupied Molecular Orbital (LUMO), and diagrams shown the Density of States (DOS). Through execution of these computations, the necessary parameters were acquired to effectively characterize the structural and electrical attributes of the models, so accomplishing objective of this study. The computer-based techniques are

valuable instruments for studying the characteristics of materials at the molecular and atomic scale, with the aim of gaining insights into their potential uses. [128-130].

4.2. URANIUM ATOM

In the second part of this study, quantum calculations conducted by using Density Functional Theory to optimize the structures models and assess their characteristics. Specifically, the calculations were executed utilizing B3LYP Exchange-Correlation Functional and the 6-31G (d) basis set through the Gaussian program [127]. Effective Core Potential (ECP) basis set with LANL08d employed for doping uranium atom, which illustrated in Figure 5.4, we get three models of uranium-doped graphene, denoted as (UG1), (UG2), and (UG3) in ascending order of surface layer size, were examined.

To analyze the electronic and structural characteristics of models, various parameters such as the energy levels of the Highest Occupied and Lowest Unoccupied Molecular Orbitals (HOMO and LUMO), Energy-Gap (EG), Fermi-Energy (FE), chemical-Hardness (H), chemical-Softness (S), and Dipole-Moment (DM) assessed and presented in Table 5.2. Additionally, the distribution patterns of HOMO-LUMO, Electrostatic Potential (ESP) Surfaces, and Density of States (DOS) diagrams for the models illustrated in Figure 5.6. This comprehensive information serves the purpose of investigating U-doped graphene models in this study.

4.3. PLUTONIUM ATOM

This study focused on investigating the (3) models of conical Nano-carbons with declination angles of 120^{o}, 180^{o}, and 240^{o}. In these models, the apex atom intentionally doped with a Plutonium atom, resulting in the targeted Plutonium -doped conical Nano-carbons (Fig. 5.7). Following the identification of stable structures, the bond strength between the Plutonium and carbon atoms analyzed using the Quantum Theory of Atoms in Molecules (QTAIM) approach (Table 5.3) [131]. Subsequently, atomic Quadrupole Coupling Constant (QCC) parameters of the Plutonium atom in the examined models assessed as shown in (Table 5.4) [132]. Moreover, electronic

features including energies of the Highest Occupied levels (HOMO) and the Lowest Unoccupied levels (LUMO), Energy-Gap (EG), Fermi-Energy (FE), Chemical-Hardness (CH), and Chemical-Softness (CS) assessed and documented in Table 5.5. Subsequently, Electrostatic Potential (ESP) surfaces and (HOMO-LUMO) distribution patterns for investigated models examined and presented in Figure 5.8. Demonstrating changes in electronic molecular orbital levels, Density of States (DOS) diagrams for the model systems illustrated in Figure 5.9. All computations conducted using the (B3LYP) level of Density Functional Theory with (6-31G*) basis set for carbon and hydrogen atoms, and the (LANL2DZ)basis set for the Pu atom, implemented through (GAMESS) program. [127, 133, 134]. It is worth to mention that the role of hydrogen atoms was to saturate the carbon atoms of the base of conical structure avoiding the existence of dangling effects [135].

PART 5

RESULTS AND DISCUSSION

5.1. LEAD-DOPED

In the initial segment of our research, density functional theory calculations were employed to analyze models of graphene doped with single and double lead atoms (Figures 5.1 and 5.2). Undoubtedly, the presence of lead (Pb) in the environment is a matter of great concern, necessitating cautious handling and management [21, 22]. Coronene was chosen as a representative model for graphene, aligning with prior research (25-27), to address the molecular-level objectives of this study. The original and lead-doped models under investigation individually optimized to achieve structures with minimal energy. These structures, together with their optimized configurations, bond lengths, and associated IR spectra, are visually presented in Figure 5.2. In the present study, the investigation focused on single and double lead -doped models of graphene through the utilization of density functional theory computations. Undoubtedly, the presence of lead (Pb) in the environment is a matter of great concern, necessitating cautious handling and management. In this situation, a visual comparison of the models is warranted since noticeable variations in their morphologies may be noted while transitioning from the original model to both the single and double lead-doped versions. It is important to highlight that the development of double-doped models included the exploration of two different configurations, specifically Cis and Trans. These configurations were determined based on the attachment of double lead atoms either to the same side or opposite sides of the coronene layer, respectively. Initial observation should be focused on the total energy outcomes presented in Table 1, which pertain to the utilization of distinct basis sets for a single lead atom in the single lead-doped model and double lead atoms in the double lead -doped models.

Therefore, the comparison of energy between various models is not relevant. However, such a comparison may be used when comparing double lead-doped models. Consequently, the assessed total energies of the double lead-doped models indicated that the Cis (same sides) conformation exhibited a somewhat higher level of stability compared to the Trans (opposite sides) conformation. When reviewing the contents of Figure 5.2, it becomes evident that the differences in bond lengths are more pronounced in the opposite sides conformation compared to the same side conformation. Consequently, the same side model exhibits more stability. Therefore, the total energies of the double lead-doped models were examined, revealing that the same side conformation exhibited a somewhat higher stability compared to the opposite sides conformation. Furthermore, the same side model was shown to have more robust IR peaks than the opposite sides model, suggesting that the same side model forms bonds more strongly. Further investigation into single and double lead-doped models, where stabilized structures were seen, may reveal the benefit of such molecular-scale coronene for taking part in dual doping by lead atoms. Bond length investigations performed with care might reveal how the presence of lead dopants alters the structural geometries, resulting in different bond lengths and forms. The lead-doped models well predicted the observed deviations from the parent structure, suggesting that structural lineaments rearranged in response to the presence of dopant atoms. Figure 5.2's content warrants more inspection, as it may reveal bond length variations, with more dramatic shifts in the Trans conformation than the Cis (same side) conformation, leading to greater stability for the same side model. Therefore, the same side conformation was shown to be somewhat more stable than the opposite sides conformation when the total energies of double lead-doped models were compared. Hence, it is essential to acknowledge the significance of including electronic aspects in these models to demonstrate the effects of structural modifications on the distinctive electronic attributes of the analyzed structures. The energy levels of the Highest Occupied Molecular Orbital (HOMO) and the Lowest Unoccupied Molecular Orbital (LUMO) are significant electronic characteristics owing to their pivotal involvement in electron transfer phenomena. Specifically, HOMO can be regarded as the electron donor level, while LUMO may be viewed as the electron acceptor level in electron transfer processes. Hence, it is crucial to investigate these levels to further the understanding and application of their respective contributions to electron transport

processes. Thus far, the examination of the Highest Occupied Molecular Orbital (HOMO) and Lowest Unoccupied Molecular Orbital (LUMO) in the optimized models has shown diverse electronic characteristics, as evidenced by alterations in these energy levels between the original and doped states. A comprehensive analysis of double lead-doped models reveals distinct variations in their electronic transfer characteristics, as well as disparities in their stability and structural attributes. The presence of lead dopants was seen to have an impact on both the structural configurations and electronic properties. The energy gap and Fermi energy values have been seen to exhibit alterations in electronic properties because of the introduction of Lead-doped models. The visual representation of ESP surfaces, HOMO and LUMO distribution patterns, and DOS diagrams in Figure 5.3 provides a descriptive account of the internal processes occurring inside the molecular system. These exhibitions provide insights into the variations seen in the molecular orbital characteristics of the models. An interesting observation regarding the Lead-doped models was the significant impact of substituting heavy metal atoms on neutralization the electrostatic charge of coronene. The replacement caused a shift from the red hue in the central area of the original model to the green shade across the entire surface of the modified models. In the aforementioned depictions, the use of the color red signifies the presence of negative electrostatic charges, whereas the color green denotes neutrality, and the color blue signifies the presence of positive electrostatic charges. The presence of a region doped with lead might potentially cause a disturbance to the electrostatic potential (ESP) characteristics of a model system of coronene. Additionally, the distribution patterns of the highest occupied molecular orbital (HOMO) and the lowest unoccupied molecular orbital (LUMO) might provide insights into the impact of lead doping on the shapes and orientations of molecular orbitals. It is seen that the introduction of lead dopant leads to considerable alterations in the morphologies of the models compared to their original counterparts. The DOS diagrams that were assessed also exhibited changes of molecular orbitals distribution for lower levels than HOMO and higher levels than LUMO. These differences appeared in diverse modes of distribution, with varying gap sizes between the two levels. The obtained findings have significance in the analysis of the electronic characteristics of the models, enabling the prediction of their potential uses in electronic settings. Notably, the lead doped models

exhibit novel properties when compared to the prototype. The Dipole Moment and Volume values indicate variations in the distribution of electric charge for the models.

The primary objective of this study was to examine the characteristics of carbon layers in relation to Lead adsorption by focusing on the presence of single and double Pb-doped models of graphene. It is anticipated that Unchangeable adsorptions of heavy metals would be more effective than reversible adsorptions in achieving removal objectives. Previous studies have revealed the feasibility of attaining Pb-doped configurations [136]. Hence, this study explores the concept of including double Pb-doped models with the already established single Lead-doped models. The models used in this study were derived as stable models for Lead-doped graphene. The stability of these models was also assessed in comparison to previous studies, demonstrating a satisfactory achievement of the research objective [126]. The examination of structural and electrical characteristics between the original and the doped models may highlight the potential of structural adjustments in achieving desired materials. The above modifications have the potential to create innovative configurations with distinctive characteristics that are well suited to a variety of applications. In the context of this study, the implementation of double doping resulted in the formation of layers that had dual functionalities in both the same side and opposite sides models.

5.2. URANIUM-DOPED

The main goal of this study was to examine the electrical and structural characteristics of U-doped analogues of graphene (UG) via the use of Density Functional Theory computations. To achieve this objective, three models investigated. They differed in the presence of carbon layers around the central Uranium-doped region. These models, namely (UG1), (UG2), and (UG3), were characterized by one, two, and three carbon layers surrounding the central region, as seen in Figure 5.4. The significance of this matter is in the examination of the impact of structural size effects on the electrical characteristics of the models, a subject that was explored in this study. Firstly, it is crucial to acknowledge that the layer structures of (UG) models were successfully attained and suitably stabilized. In order to investigate electronic characteristics, the

aforementioned structures were used in novel computations aimed at assessing the necessary data for understanding the models based on electronic descriptors. As shown by the data presented in Table 5.2, a concise summary of frontier molecular orbitals information was provided, with particular emphasis on the significance of the Highest Occupied Molecular Orbital (HOMO) and the Lowest Unoccupied Molecular Orbital (LUMO) as key properties at the molecular level. These two levels play a crucial role in determining the characteristics of the electronic transfer process, serving as a significant component in identifying the conductivity function of materials. The HOMO is involved in electron donation, whereas the LUMO is involved in electron acceptance. Consequently, the determination of energy gaps between these two states has significant importance in the identification and understanding of internal electron transfer occurring between them. Consequently, a meticulous examination of the highest occupied molecular orbital (HOMO) and lowest unoccupied molecular orbital (LUMO) has the potential to provide valuable insights into the electronic conductivity of the UG models under investigation. The impacts of structural sizes on the energy levels of UG models (Figure 5.5) were noticed by the analysis of HOMO and LUMO levels, as shown by the content of Table 5.2. In this context, it is seen that the HOMO level experienced a small alteration between UG1 and UG3. Conversely, the LUMO level underwent a predominant shift from UG1 to UG3, transitioning from a lower energy state to a higher energy state. Consequently, the energy gap between the highest occupied molecular orbital (HOMO) and the lowest unoccupied molecular orbital (LUMO) was seen to be less for (UG3) model when compared to the previous (UG1) and (UG2) models, thereby confirming the influence of size on electronic characteristics. The Energy Gap (EG), and Inferred have relation to the change of the Highest Occupied Molecular Orbital (HOMO) and Lowest Unoccupied Molecular Orbital (LUMO), wherein lower EG values equate to a greater conductivity function for the material under investigation. In support of this accomplishment, the FE values indicate that the UG3 model exhibits a greater ease in reaching the Fermi level compared to the UG1 and UG2 models, hence highlighting the significant role of molecule size in attaining conductivity functionality. Nevertheless, it should be noted that increased conductivity is not always advantageous, since there are instances when being a semiconductor might actually be beneficial for sensing applications. In the context of diagnostic applications, the manipulation of energy gaps between the

highest occupied molecular orbital (HOMO) and the lowest unoccupied molecular orbital (LUMO) levels holds potential for the creation of materials that exhibit desired conductive or semi-conductive properties. These properties are of significant importance for the development of industrial devices, including those utilized in the field of biomedical diagnostics and sensing. [137-139].

Based on the acquired accomplishments, it has been observed that molecules of smaller dimensions exhibit properties akin to semiconductors, whereas molecules of larger dimensions exhibit properties like to conductors. The examination of Chemical Hardness and Softness values (H and S) further confirmed increased reactivity for UG3 and decreased reactivity for (UG1) by a comparison of the respective (H) and (S) characteristics. Higher magnitude of (H) indicate more reluctance to participate in reactions with other chemicals, whereas higher magnitude of (S) indicate a greater propensity to participate in reactions, and versa vice. Consequently, the reactivity mode was adjusted based on the fluctuations of the Highest Occupied Molecular Orbital (HOMO) and Lowest Unoccupied Molecular Orbital (LUMO) levels in order to attain suitable characteristics corresponding to the sizes of the models under investigation. Figure 5.5 displayed the assessed distribution patterns of the Highest Occupied Molecular Orbital (HOMO) and lowest unoccupied molecular orbital (LUMO). Furthermore, the electrostatic potential (ESP) surfaces for the (UG1), (UG2), and (UG3) models were also shown. The quantitative measurements of the Highest Occupied Molecular Orbital (HOMO) and lowest unoccupied molecular orbital (LUMO) indicate that the changes in the LUMO are more pronounced compared to those in the HOMO. This observation is supported by the observed distribution patterns. The HOMO patterns exhibited a high degree of similarity across the (UG1), (UG2), and (UG3) models, suggesting a nearly comparable electron-donating characteristic throughout all model systems. Nevertheless, the LUMO patterns exhibited notable alterations from (UG1) to (UG3), indicating the changes in electron acceptance characteristics across the models due to size effects. It could be reasonable to infer that models may be classify based on their electron accepting characteristics. Specifically, the LUMO levels in the vicinity of the U-doped area play a crucial role in determining this functionality for the models under investigation. The ESP surfaces also revealed that the primary factor influencing the electrical properties

of the models under investigation is the U-doped area. This region, shown by the blue hue, is believed to play a central role in the diagnostic functions of the models being studied. It is noteworthy to acknowledge that atomic dopant models have the potential to be applicable in atomic adsorption methods using graphene layers. This additional benefit highlights the advantages of utilizing nanostructures for the purpose of removing pollutants from the environment [140-142]. Consequently, the examination of the structural stability of the examined (UG) models, together with the assessment of their electrical properties, may contribute to the advancement of graphene applications in the form of Uranium-doped models. The DOS diagrams shown in Figure 5.6 provide more evidence of the electrical characteristics pertaining to the HOMO and LUMO energy levels. Specifically, the Density of States diagrams indicate that the HOMO and LUMO levels of UG3 exhibit a significant degree of overlap, resulting in enhanced conductivity for this particular model when compared to UG1 and UG2.

5.3. PLUTONIUM-DOPED

In this study, the electrical and structural properties of three Pu-doped conical Nano-carbons, namely PuNC120, PuNC180, and PuNC240, were examined. Figure 5.7 displays these models, each possessing declination angles of 120, 180, and 240 degrees, respectively. The Pu-doped atom located at the apex of the conical structure determined to engage in 4, 3, and 2 chemical bonds. The stabile model discovered to have varying distances of Plutonium-Carbon bonds near the tip of conical shapes. Consequently, an assessment of the QTAIM characteristics was conducted to analyze the chemical bonds in question. The strength of the Pu-C bonds in Table 5.3 indicates their ability to form chemical compounds. However, it is noteworthy that the strength of these bonds varied within the same model, in addition to the observed variances among different models. Thus far, the determined magnitudes of Bond Critical Points (BCP) for the Plutonium-Carbon bonds, namely the total Charge Density (ρ), Laplacian of Charge Density ($\nabla^2\rho$), and Electron Energy Density (H), have served as indicators of the formation of distinct chemical bonds. The above values have been used to examine the Pu-C bonds within a single model and to perform a comparative analysis of the Pu-C bonds in three different models. The findings obtained in this

study provide confirmation of the presence of varying lengths between Pu-C bonds in the models that were examined. The bonds with the shortest distances, indicating stronger bonding, were detected in the PuNC120 models. The average values of the parameters in Table 5.3 show that the PuNC180 and PuNC240 models came next. According to the QCC values of the Pu atom (see Table 5.4), the electronic environment of the Plutonium atom had a bigger influence on the electronic environments of the adjacent Carbon atom. The QCC properties were analyzed, revealing that the Plutonium atom of (PuNC120) model exhibited the lowest value. Similar observations regarding bond strength were made for the (PuNC180) and (PuNC240) models. The models were subjected to additional analysis using the obtained results of electronic molecular orbitals, which included the values of HOMO (Highest Occupied Molecular Orbital), LUMO (Lowest Unoccupied Molecular Orbital), EG (Energy Gap), FE (Frontier Electron Density), CH (Chemical Hardness), and CS (Chemical Softness). This analysis was complemented by visual representations of (Electrostatic Potential) ESP surfaces, distribution patterns (HOMO-LUMO), and (Density of States) DOS diagrams (as shown in Table 5.4 and Figures 5.8 and 5.9). During this stage, we collected both quantitative and qualitative findings to identify the electrical and conductivity characteristics of the researched models, with the aim of demonstrating the advantages of including a doping Pu atom in the conical model. Based on the results of the Quantum Theory of Atoms in Molecules (QTAIM) research, it was seen that the Plutonium -Carbon bonds in the (PuNC120) model exhibited more strength compared to the other two models. Additionally, the blue area around the Plutonium atom located at the apex of the conical structure was found to be somewhat smaller in size when compared to the other two models. This visual representation might potentially demonstrate a greater degree of interaction between the electronic environment of a Plutonium atom and the electronic environments of the adjacent Carbon atoms. Consequently, a minute blue region corresponding to the Plutonium atom and a broader green region corresponding to the Carbon atoms detected. In contrast to this particular mode, the displayed electron density surfaces of the other two models exhibited more vibrant colorations, which suggest a lesser influence of the electronic surroundings of the plutonium atom in relation to the surrounding carbon atoms. Additional comprehensive findings may be gained by the examination of the observed distribution patterns of the highest occupied

molecular orbital (HOMO) and lowest unoccupied molecular orbital (LUMO), as well as the quantitative data shown in Table 3. These results, in conjunction with the diagrams of the density of states (DOS) depicted in Figure 5.9, provide a more thorough understanding of the researched models. The PuNC120 model exhibited broader distribution patterns of HOMO-LUMO, indicating a greater abundance of these electronic molecular orbitals compared to the PuNC180 and PuNC240 models. Based on the above results, it is evident that the quantitative measurements of the highest occupied molecular orbital (HOMO) and the lowest unoccupied molecular orbital (LUMO) exhibit disparities throughout the models under investigation. Particularly, the PuNC120 model had the smallest energy gap (EG) between the HOMO and LUMO levels among the models examined. In the PuNC180 and PuNC240 models, the LUMO level was elevated, resulting in an increase in the distance as seen by the EG values. Furthermore, it was also noted that there were fluctuations in the values of FE, which suggests alterations in the characteristics of electronic conductivity. The molecular orbital fluctuations were shown in the illustrated diagrams of DOS, as presented in Figure 5.9. The models exhibited varying levels of CH and CS. The puNC120 model used as the predominant model in this study, with the anticipation that derived CH and CS values would facilitate the understanding of its impact on other chemical processes. Undoubtedly, lower levels of hardness and higher levels of softness have the potential to provide more favorable outcomes in the context of chemical reaction systems. As a result, the models were acknowledged for their ability to demonstrate diverse electrical functionalities that meet the unique requirements of applications across numerous domains, in accordance with the predetermined standards.

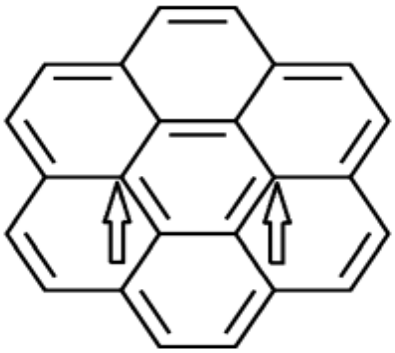

Figure 5.2. Coronene Structure ; arrows indicate the Pb-doped sites.

Side View/ Original > Bond Lengths Å IR Spectra

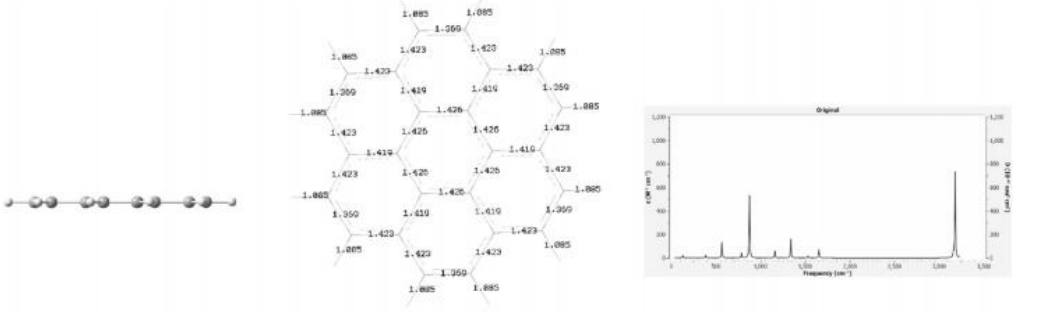

Single Pb-Doped >

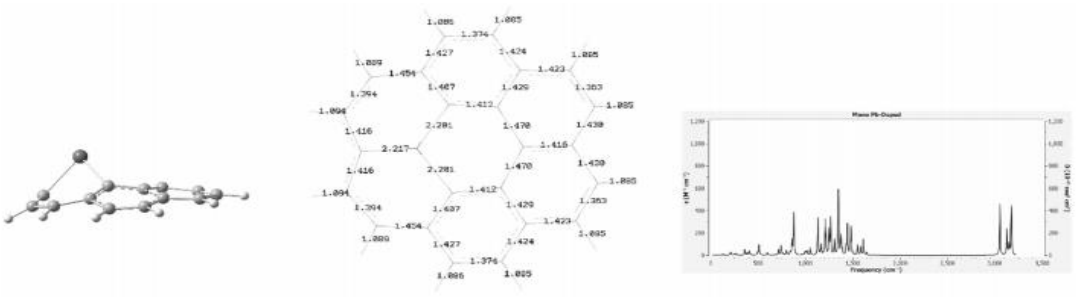

Double Pb-Doped Cis >

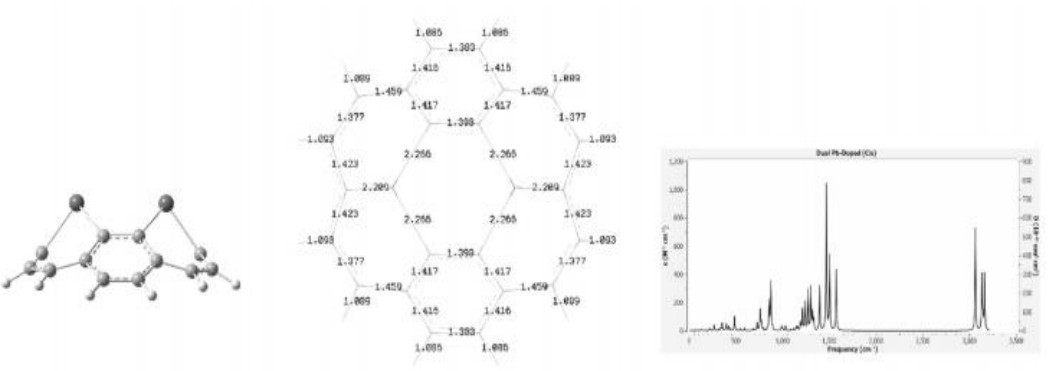

Double Pb-Doped Trans >

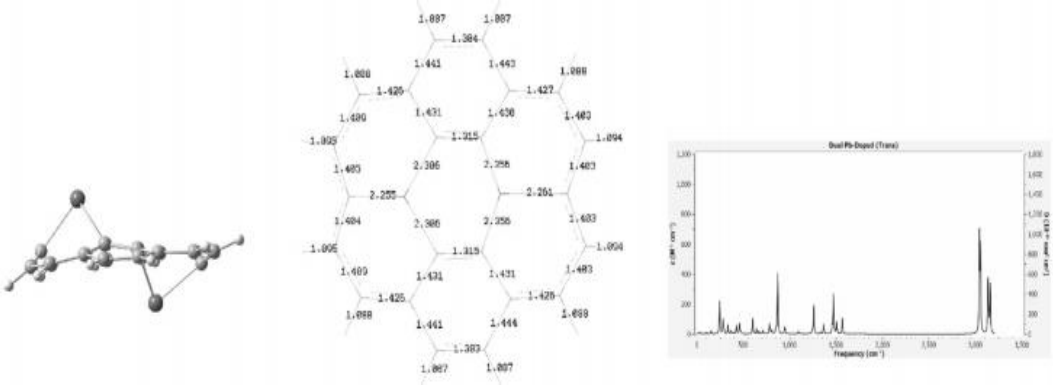

Figure 5.3. IR spectra Side-views, and bond lengths for lead doped models.

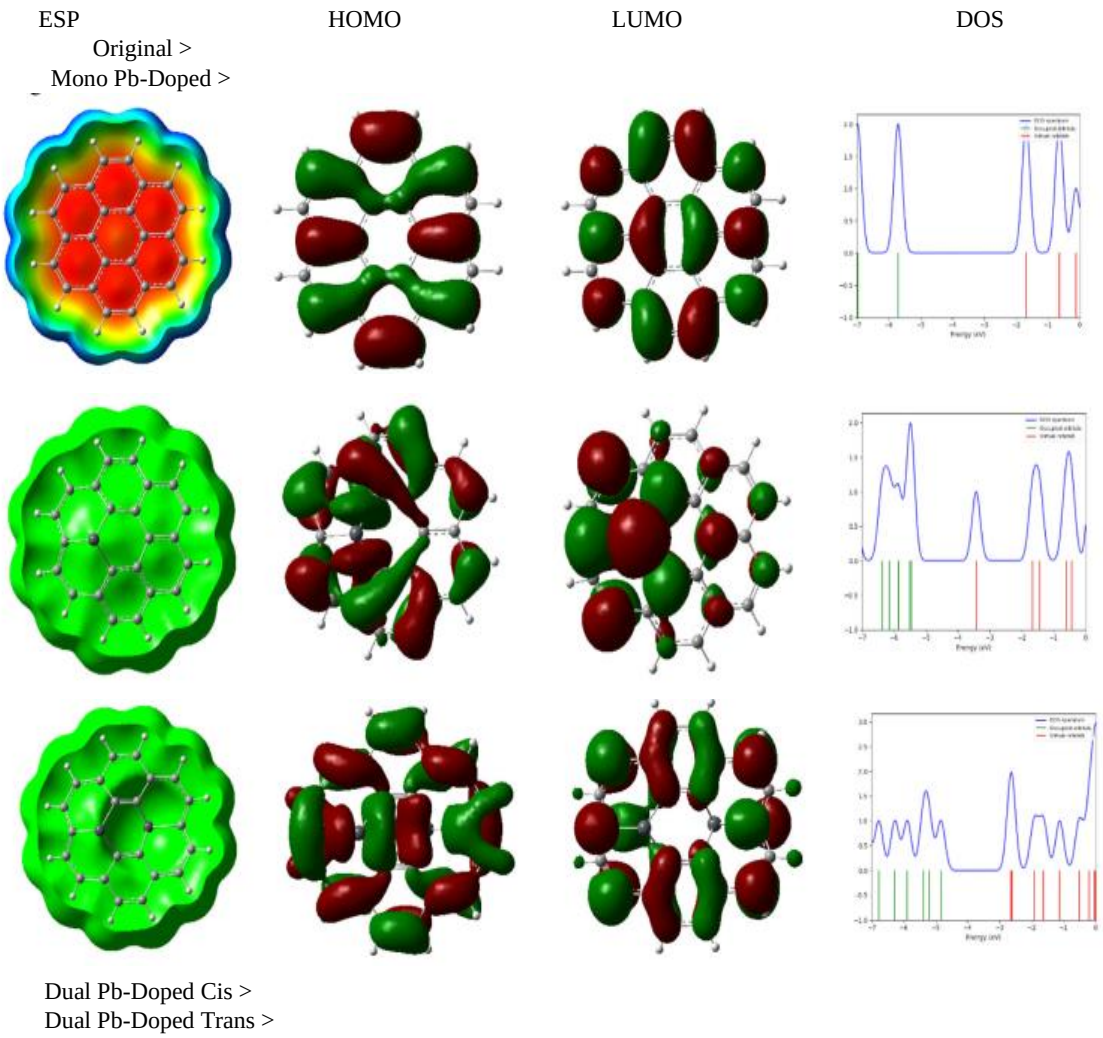

Figure 5.4. DOS diagrams, HOMO, LUMO energy level patterns and ESP surfaces.

Table 5.1. Features Optimiztion for lead doped models.

Feature	Original	Single lead-Doped	Double lead-Doped Cis	Double lead-Doped Trans
E(eV)	-25,091.999	-24,143.568	-23,197.651	-23,196.233
HOMO(eV)	-5.707	-5.467	-5.094	-4.832
LUMO(eV)	-1.683	-3.427	-3.819	-2.653
EG(eV)	4.024	2.040	1.275	2.179
FE(eV)	-3.695	-4.447	-4.142	-3.742
DM(Debye)	0	1.562	3.660	1.518
V(cm^3/mole)	230.497	262.465	261.085	266.012

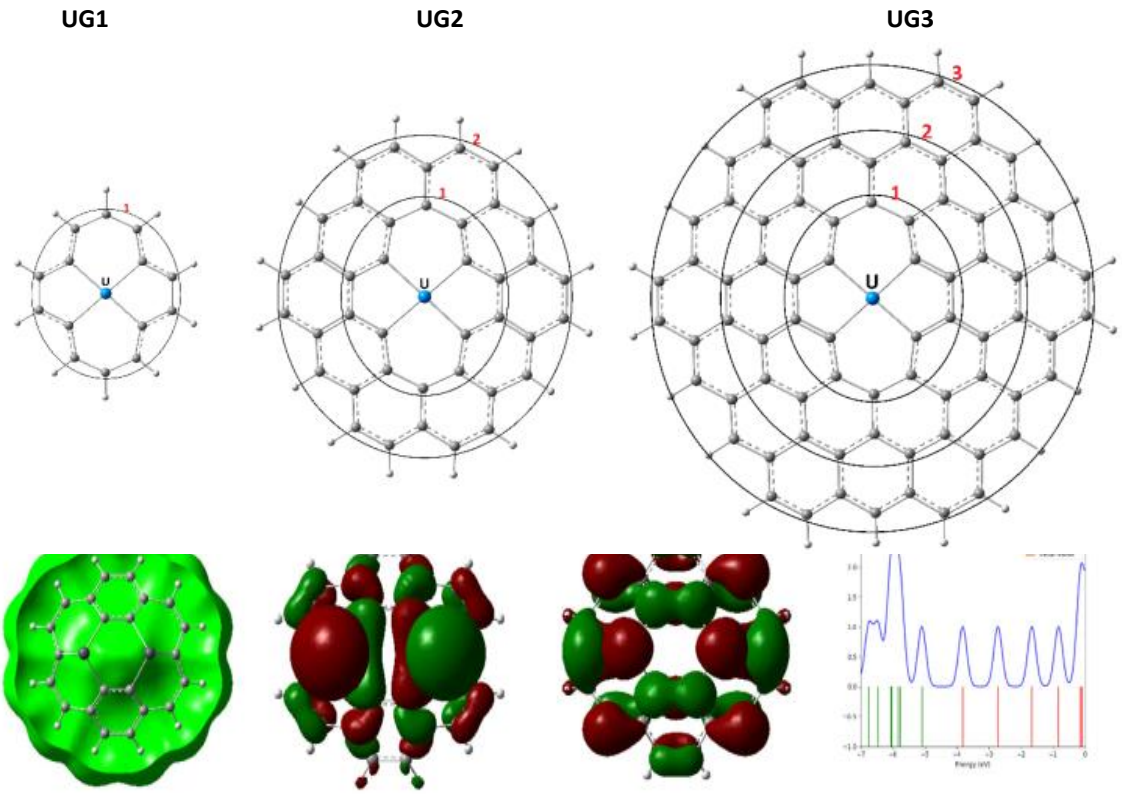

Figure 5.5. The Uranium-doped models of graphene (UG). Circles show number of surrounding carbon layer around the central Uranium atom.

Table 5.2. Features of Uranium-doped molecules.

Feature	**(UG1)**	**(UG2)**	**(UG3)**
HOMO(eV)	**-3.45**	**-3.17**	**-3.57**
LUMO(eV)	**-1.90**	**-2.09**	**-2.73**
EG(eV)	**1.56**	**1.07**	**0.84**
FE(eV)	**-2.68**	**-2.63**	**-3.15**
H(eV)	**0.78**	**0.54**	**0.42**
S(eV)$^{-1}$	**1.29**	**1.86**	**2.37**

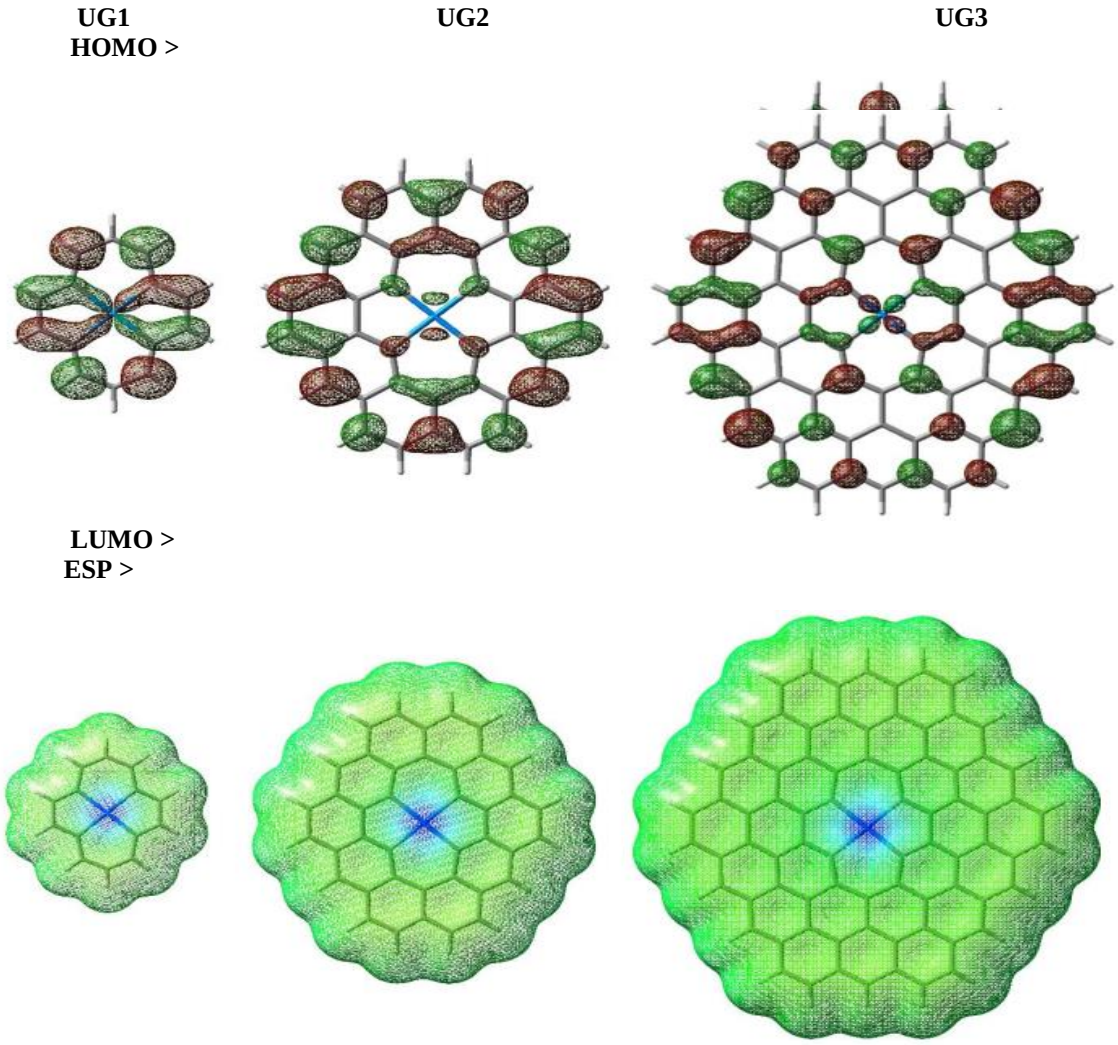

Figure 5.6. ESP surfaces and HOMO, LUMO energy level patterns of Uranium-doped models for graphene (UG).

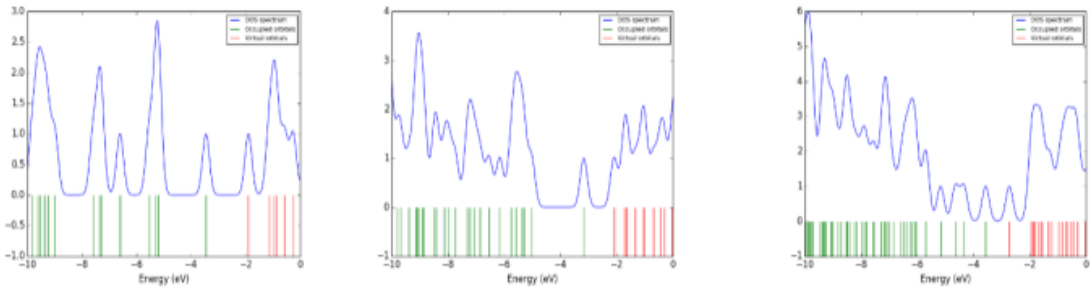

UG1 UG2 UG3

Figure 5.7. Density of statse diagrams for the Uranium-doped models of graphene.

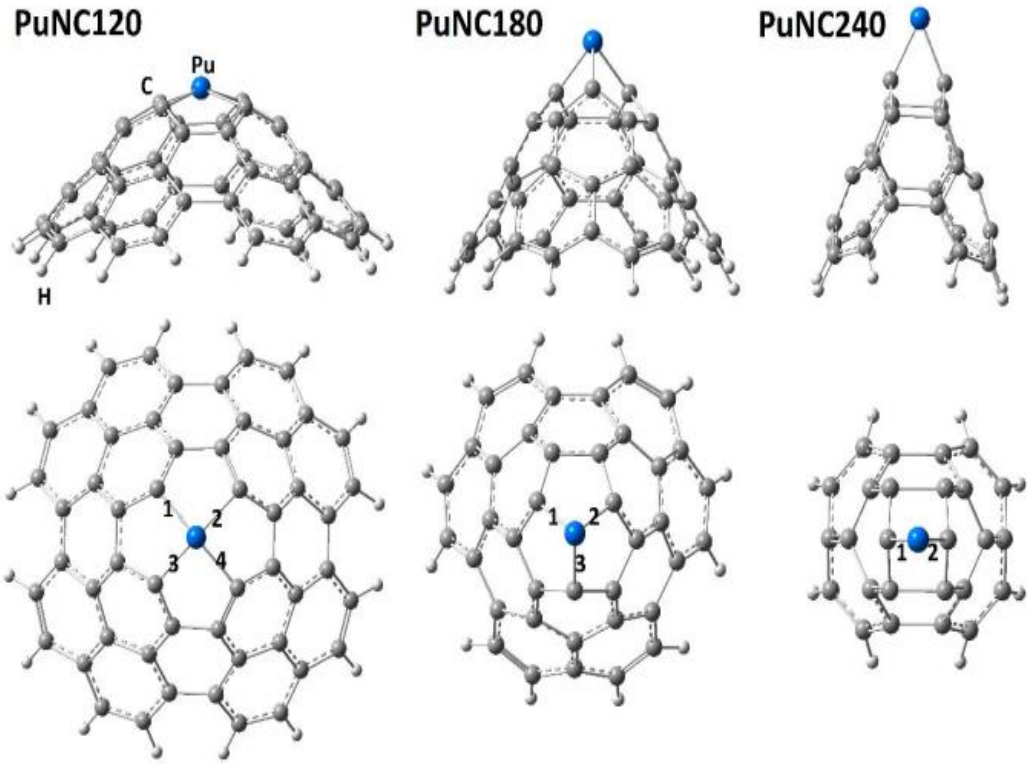

Figure 5.8. Different Plutumium doped model represented by PuNC120, PuNC180, and PuNC240 models.

Table 5.3. The QTAIM analysis resulte of Pu-C bonds.*

Model	Bonds	D	ρ	$\nabla^2\rho$	H
PuNC120	1	1.855	0.2574	-0.2469	0.2202
	2	1.953	0.2092	-0.0856	-0.1495
	3	1.858	0.2545	-0.2025	-0.2159
	4	1.946	0.2132	-0.0791	-0.1548
Average		1.903	0.2336	-0.1534	-0.1851
PuNC180	1	1.909	0.2311	-0.0776	-0.1794
	2	1.913	0.2303	-0.0783	-0.1785
	3	1.919	0.2202	-0.0554	-0.1647
Average		1.914	0.2272	-0.0277	-0.1742
PuNC240	1	1.916	0.2231	-0.023518	-0.1721
	2	1.918	0.2202	-0.031895	-0.1681
Average		1.916	0.2216	-0.0277	-0.1701

*Please see Fig. 5.7 for Pu-models and the bonds numbers. The magnitudes of distances are in angstrom, atomic unit ρ, $\nabla^2\rho$, and H.

Table 5.4. The values of QCC feature. *

Feature	PuNC120	PuNC180	PuNC240
QCC of Pu	210.769	252.844	317.937

*Please see Fig. 5.7 for Pu-model. The units are in MHz.

Table 5.5. The Electronic Molecular Orbital Features of Pu-doped model. *

Model	HOMO	LUMO	EG	FE	CH	CS
PuNC120	-4.026	-3.164	0.862	-3.595	0.431	2.321
PuNC180	-4.291	-2.796	1.495	-3.544	0.748	1.337
PuNC240	-4.446	-2.412	2.034	-3.429	1.017	0.983

*Please see Figs. 5.7-9 for Pu-models. The magnitudes are in eV with the exception for CS which is in eV^{-1}.

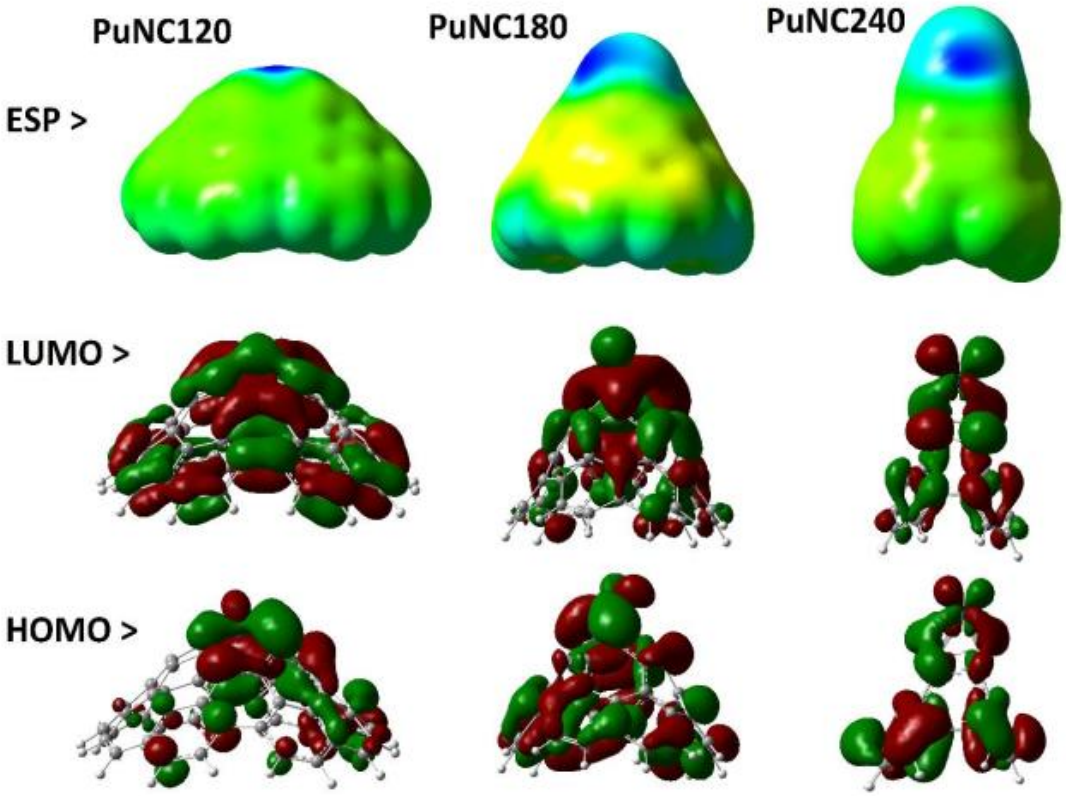

Figure 5.9. HOMO, LUMO energy level patterns and ESP surfaces of the Pu-doped models (PuNC120, PuNC180, and PuNC240).

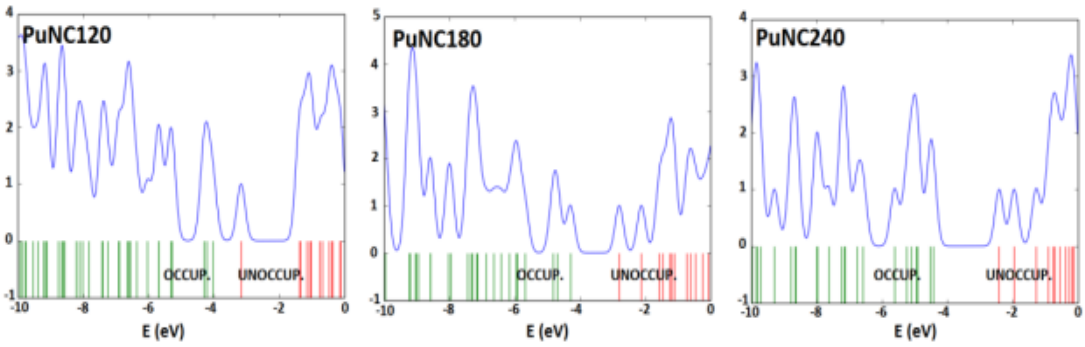

Figure 5.10. Density of states diagrams of Pu-doped models (PuNC120, PuNC180, and PuNC240).

PART 6

CONCLUSION

In this work, the electronic and molecular properties of lead, uranium and plutonium heavy metal doped graphene were investigated by the density functional theory approach. The results obtained are compiled below for each heavy metal.

6.1. LEAD MODELS

The current study aimed to evaluate the structural and electrical characteristics of single- and double Pb-doped models of graphene. This was achieved by conducting Density Functional Theory calculations on a typical coronene model. The models consisted of prototype, single Lead-doped, and double Lead-doped same side (Cis) and opposite sides (Trans) configurations. The optimization of each model was conducted individually in order to get an energy structure with minimized values. This minimized energy structure was then validated by frequency calculations, ensuring the absence of any imaginary frequency. Subsequently, an assessment was conducted on the electronic characteristics of the optimized models, revealing notable impacts of Pb-doping on the electronic properties of the models and the presence of structural variations. The research results of the study revealed that all models with Pb-doping were effectively stabilized, with the same side double Lead-doped model demonstrating superior performance compared to the opposite sides model. Consequently, the analyzed infrared spectra likewise exhibited more pronounced peaks for the same side model. The orbit of molecule characteristics were shown to be significantly influenced by the presence of Lead dopants in the models. The presence of the Pb dopant resulted in alterations to both the energy levels and the morphologies of the highest occupied molecular orbital (HOMO) and the lowest unoccupied molecular orbital (LUMO). Additionally, the DOS diagrams showed differences in the characteristics of the Highest Occupied Molecular Orbital and the Lowest Unoccupied

Molecular Orbital. Consequently, these models were chosen for future application development because of their distinctive structural and electrical characteristics.

6.2. URANIUM MODELS

We investigated to examine the electrical and structural characteristics of Uranium-doped forms of graphene, namely (UG1), (UG2), and (UG3) models. These models were distinguished by varying widths of the carbon layer around the center Uranium-doped area. The density functional theory computations were conducted to acquire stabilized structures and assess the corresponding electrical characteristics. Based on the acquired accomplishments, it can be say that the models successfully stabilized, and the influence of size on the determination of electrical characteristics was readily apparent. The larger model (UG3) exhibited a greater level of conductivity in comparison to the smaller model (UG1), thus confirming the influence of size on electrical characteristics. The observation indicated that the impact was more pronounced on the (LUMO) level compared to the (HOMO) level, implying that the electron acceptance propensity of the models exhibited considerable alterations across varying sizes. Therefore, this suggested feature aims to facilitate the development of new sensor materials by using the explored (UG) models.

6.3. PLUTONIUM MODELS

This section examines the structural and electrical characteristics of all three types of Plutonium-doped conical Nano-carbons, namely (PuNC120), (PuNC180), and (PuNC240). The findings of the study revealed that the characteristics of the models were contingent on the disclamation angles. Specifically, the model with an angle of 120^{o} exhibited a substantial distinction from the other two models, which had angles of 180 and 240 degrees. The characteristics of the models that observed suggest that the PuNC120 model exhibits stronger Plutonium-Carbon bonds, as seen by the shorter gap between the HOMO and LUMO levels compared to the other models. In conclusion, this study has shown that the electrical and conductivity properties of the specified applications may be modulated by the specifications of the structures (conical) and the presence of the doping Pu atom.

PART 7

SUMMARY

The advent of graphene and nanostructures and their distinctive properties over more than twenty years has given a new and exciting movement to the study of materials. Where the machine learning methods (electronic techniques) enabled the simulation of the molecule to obtain its electronic, optical, and structural properties, such as energy gaps, bond lengths between atoms, and formation energies for its different doped systems. The density functional theory has been employed as a good tool to obtain these properties, and to reinforce them with other materials for industrial, medical, and environmental purposes, as it is possible to rely on the theoretical results obtained from this theory to carry out practical tests for them. Currently, it can be said that the computational density functional theory technique has made a great contribution to materials design along with its practical application. So, the computational concepts and modeling have become more complex. Graphene, nanostructures, and their remarkable properties have also become the focus of research by many researchers. The fact that the surface of graphene and nanostructures are a substrate for achieving chemical reactions, and the absorption of other materials has become an application to remove environmental pollutants, or to deliver drugs to the human body. In addition to the distinctive electronic role as a semiconductor material and other applications that can be verified theoretically by using DFT approach before being verified practically.

In this work, a surface was prepared for the adsorption of some radioactive materials, such as lead, uranium, and plutonium. Using the theoretical density function, and theoretical calculations made to calculate the HOMO and LUMO energy. In order to obtain miniature energy structures, molecular and atomic properties, as well as DOS diagrams as results of adsorption of lead, uranium and plutonium, where the necessary improvements have been successfully made in order to obtain a better electronic

modeling, which has been evaluated, may contribute to other advanced applications of these models.

For lead (Pb) adsorption, three models used for the adsorption of one (single) or two (double) atoms and on same side (Cis) or on opposite sides (Trans) across a coronene molecule. Graphene with three sizes around the central uranium molecule used to obtain three layers of UG1, UG2 and UG3, and screened to obtain the most stable composition of the electronic structure.

In the case of single- and double Pb-doped models, the conformational arrangements of same side and opposite are established by positioning two Pb atoms on the same side of the graphene structure in the Cis model and by putting two Pb atoms on opposing sides in the Trans model. Three sizes of models investigated based on the number of surrounding layers around the U-doped central region including UG1, UG2 and UG3. Finally, three conical Nano-carbon models with detection angles of 120, 180 and 240 degrees were investigated, in which a plutonium atom was doped at the apex of the conical structure.

REFERENCES

1. Younis S. A., Maitlo H. A., Lee J. and Kim K. H., "Nanotechnology-based sorption and membrane technologies for the treatment of petroleum-based pollutants in natural ecosystems and wastewater streams", ***Adv. Colloid Interface Sci.***, 275 102071 (2020).

2. Tran N. H., Le B.H., Zhao S., and Mi Z., "On the mechanism of highly efficient p-type conduction of Mg-doped ultra-wide-bandgap AlN Nanostructures". ***Applied Physics Letters***, 110 032102 (2017).

3. He S., Chen G., Xiao H., Xiao Ch., Ma Y., Dai H., Yuan B., Chen X., Yang X., "Facile preparation of *N*-doped activated carbon produced from rice husk for CO_2 capture", ***J. Colloid Interface Science***, Vol. 582, Part A, Pages 90-101 (2021).

4. Ji Q., Hu C., Liu H., and Qu J., "Development of nitrogen-doped carbon for selective metal ion capture", ***Chem. Eng. J.***, 350 608 (2018).

5. Yang, Z.; Tian, J.; Yin, Z.; Cui, C.; Qian, W.; Wei, F.," Carbon nanotube- and graphene-based nanomaterials and applications in high-voltage super capacitor: A review", ***Carbon***, 141, 467–480 (2019)**.**

6. Fedorov A. G., "Prediction of the structure of non-carbon nanotube WS_2", ***AIP Conf. Proc.***, 2041 040004 (2018).

7. Yang G., Li L., Lee W.B., and Ng M. Ch.,"Structure of graphene and its disorders: a review", ***Science and Technology of Adv. Mater.***, Vol.19, 613 (2018).

8. Xu J., Cao Z., Zhang Y., Yuan Z., Lou Z., Xu X., and Wang X., "A review of functionalized carbon nanotubes and graphene for heavy metal adsorption from water: Preparation, application, and mechanism", ***Chemosphere***, Volume 195, Pages 351-364 (2018).

9. Zhang M., Zhang L., Tian Sh., Zhang X., Guo J., Guan X., and Xu P. "Effects of graphite particles/$Fe3^+$ on the properties of anoxic activated sludge", ***Chemosphere***, 253 126638 (2020).

10. Promthong N., Tabtimsai C., Rakrai W., and Wanno B., "Transition metal-doped graphene Nano flakes for CO and CO_2 storage and sensing applications: a DFT study", ***Structural Chemistry*** volume 31, pages2237–2247 (2020).

11. W Tian, W Li, W Yu and X Liu, "A Review on Lattice Defects in Graphene: Types, Generation, Effects and Regulation", ***Micro machines***, 8(5), 163, (2017).

12. Huang D., Wu J., Wang L., Liu X., Meng J., Tang X., Tang C., and Xu J., "Novel insight into adsorption and co-adsorption of heavy metal ions and an organic Pollutant by magnetic graphene Nanomaterial in water". ***Chemical Engineering Journal***, 358: 1399-1409, (2019).

13. Li Z., Peng M., Zhou X., Shin K., Tunmee S., Zhang X., Xie C., Saitoh H., Zheng Y., Zhou Z., and Tang Y., "In situ chemical lithiation transforms diamond-like carbon into an Ultra strong ion conductor for dendrite-free lithium-metal anodes", ***Advanced Material***, 33(37):2100793, (2021).

14. R Chen, Cheng Y., Wang P., and Wang Q., Enhanced removal of Co(II) and Ni(II) from high-salinity aqueous solution using reductive self-assembly of three-dimensional magnetic fungal hyphal/graphene oxide nanofibers, ***Science of The Total Environment***, 756(2) : 143871,(2020).

15. Zhang X., Tang Y., Zhang F., and Lee C-S., "A Novel Aluminum–Graphite Dual-Ion Battery", ***Adv. Energy Mater.,*** 6, 1502588, (2016).

16. Zhang M., Song X., Ou X., and Tang Y**.,** "Rechargeable batteries based on anion intercalation graphite cathodes", ***Energy Storage Mater.***, 16, 65 (2019).

17. Yang K., Liu Q., Zheng Y. and Yin H., "Locally ordered graphitized carbon cathodes for high-capacity dual-ion batteries", ***chime.*** , 60 6326 (2021)

18. H Cheng, T Li, X Li, J Feng, T Tang and D Qin, "Facile Synthesis of Co_9S_8 Nano cages as an Electrochemical Sensor for Lute Olin Detection", ***Journal of The Electrochemical Society***, Vol. 168, No. 8, (2021).

19. Luo G., Zhang Q., Min Li, Chen K., Zhou W., Luo Y., Li Z., Lu Wang, Zhao L., The K.S., and Jiang Z., "A flexible electrostatic Nano generator and self-powered capacitive sensor based on electro spun polystyrene mats and graphene oxide films", ***Nanotechnology***, Vol.32, No.40, (2021).

20. Fallahpour F., and Ariaei S., "Computational Investigation of B_6 Particle for H_2S Capturing", ***Journal of Science and Engineering,*** Vol. 2, no 1, (2021).

21. X Yang, N Guo, Y Yu, H Li, H Xia and H Yu," Synthesis of magnetic graphene oxide-titanate (TiO_3) composites for efficient removal of Pb(II) from wastewater: Performance and mechanism", ***J. Environ. Manage.*** 256 109943 (2020).

22. Baruah B. S. and Biswas R., "An optical fiber-based surface Plasmon resonance technique for sensing of lead ions: A toxic water pollutant," ***Opt. Fiber Technol.***, vol. 46, pp. 152–156, (2018).

23. Ma J., Sun Y., Zhang M., Yang M., Gong X., Yu F., and Zheng J., "Comparative study of graphene hydrogels and aerogels reveals the important role of buried water in pollutant adsorption", ***Environmental science & technology***, 51 (21), 12283-12292,(2017).

24. Thakur K., and Kandasubramanian B., "Graphene and Graphene Oxide-Based Composites for Removal of Organic Pollutants: A Review", ***J. Chem. Eng. Data,*** 64,3, 833-867 (2019).

25. Shao Y., Liu Z.L., Cheng C., Wu X., Liu H., Liu C., Wang J., Zhu S.Y., Wang V., Shi D.X., Ibrahim K., Sun J., Wang Y., and Gao H.J., "Epitaxial growth of flat antimonene monolayer: a new honeycomb analogue of graphene", ***Nano Lett.***, 18 2133 (2018).

26. Harismah K., Mirzaei M., and Moradi R., "DFT Studies of Single Lithium Adsorption on Coronene", ***Journal Zeitschrift für Naturforschung A***, 73 685 (2018).

27. Moezi, E.; Mirzaei, M., "Graphene scaffold for tioguanine delivery: DFT approach", **Lab-*in-Silico***, 2, 25- 29, https://doi.org/10.22034/labinsilico21021025, (2021).

28. Fawcett E., and Trotter J.**,** "The crystal and molecular structure of coronene", ***Royal Society***, Volume 289,Issue 1418, (1966).

29. Dong R., Pfeffermann M., Skidin D., Wang F., Fu Y, Narita A., Tommasini M., Moresco F., Cuniberti G.,Berger R., Müllen K., and Feng X., "Persulfurated Coronene: A New Generation of Sunflower", ***J. Am. Chem. Soc.*** 139, 6, 2168–2171, (2017).

30. Rani A., Reddy R., Sharma U., Mukherjee P., Mishra P., Kuila A., Sim L.C., and Saravanan P., "A review on the progress of nanostructure materials for energy

harnessing and environmental remediation." ***Journal of Nanostructure in Chemistry***, 8 255-291(2018).

31. Kasani S., Curtin K., and Wu N.,"A review of 2D and 3D Plasmonic Nanostructure array patterns: fabrication, light management and sensing applications." ***Nano photonics,*** 8, 2065-2089, (2019).

32. Mirzaei M., and Giahi M. "Computational studies on boron nitride and boron phosphide nanotubes: density functional calculations of boron-11 electric field gradient tensors". ***Physica***, E: Low-dimensional Systems and Nanostructures 42 1667-1669(2010).

33. Tiwari S.K., Sahoo S., Wang N., and Huczko A., "Graphene research and their outputs: status and prospect." Journal of Science: ***Advanced Materials and Devices***, 5 10-29(2020).

34. Lin L., Peng H., and Liu Z., "Synthesis challenges for graphene industry." ***Nature Materials***, 18 520- 524(2019).

35. Sun Z., Fang S., and Hu Y. H.. "3D Graphene materials: From understanding to design and synthesis control." ***Chemical Reviews***, 120 10336-10453(2020).

36. Naz M.Y., Irfan M., Shukrullah S., Ahmad I., Ghaffar A., Niazi U.M., Rahman S., Jalalah M., Alsaiari M.A., and Khan M.K.A., “Effect of microwave plasma treatment on magnetic and photocatalytic response of manganese ferrite nanoparticles for wastewater treatment.” ***Main Group Chemistry*** 20 423-435(2021).

37. Moezi E., and Mirzaei M.. “Graphene scaffold for tioguanine delivery: DFT approach.”, ***Lab-in-Silica,*** 2 25-29(2021).

38. Yaraghi A., Ozkendir O.M., and Mirzaei M., “DFT studies of 5-fluorouracil tautomer on a silicon graphene Nano sheet.”, ***Super lattices and Microstructures***, 85: 784-788, (2015).

39. Sen P., Nwahara N., and Nyokong T. "Photodynamic antimicrobial activity of Benz imidazole substituted Phthalocyanine when conjugated to nitrogen doped graphene quantum dots against staphylococcus aureus." ***Main Group Chemistry***, 20 175-191(2021).

40. Hu J., Lin W., Lin B., Wu K., Fan H., and Yu Y.. "Persistent DNA methylation changes in zebrafish following graphene quantum dots exposure in surface chemistry-dependent manner." ***Ecotoxicology and Environmental Safety***, 169 370-375(2019).

41. Kaplan A., Yuan Z., Benck J.D., Rajan A.G., Chu X.S., Wang Q.H., and Strano M. S. "Current and future directions in electron transfer chemistry of graphene." ***Chemical Society Reviews,*** 46 4530-4571(2017).

42. Assadi M.G., Ziaei M., and Rezaii E. "Synthesis of some silyl derivatives of graphene oxide." ***Main Group Chemistry,*** 20 119-132, (2021).

43. Mirzaei M. "Calculation of chemical shielding in C-doped zigzag BN nanotubes." ***Monatshefte für Chime-Chemical Monthly***, 140 1275, (2009).

44. Mirzaei M., Mirzaei M., "Sulfur doping at the tips of (6, 0) boron nitride nanotube: a DFT study." ***Physica E: Low-dimensional Systems and Nanostructures***, 42 2147-2150 (2010).

45. Mirzaei A., Kwon Y.J., Wu P., Kim S.S., and Kim H.W. "Converting the conducting behavior of graphene oxides from n-type to p-type via electron-beam irradiation." ACS ***Applied Materials & Interfaces***, 10 7324-7333(2018).

46. Rao C.N.R., Gopalakrishnan K., and Govindaraj A. "Synthesis, properties and applications of graphene doped with boron, nitrogen and other elements." ***Nano Today***, 9 324-343(2014).

47. Cui Y., Zhang R., Zhang J., Wang Z., Xue H., Mao W., and Huang W., "Highly active and stable electro catalytic hydrogen evolution catalyzed by nickel, iron doped cobalt disulfide@ reduced graphene oxide Nano hybrid electro catalysts." ***Materials Today Energy***,7 44-50(2018).

48. Kaur M., Kaur M., and Sharma V.K. "Nitrogen-doped graphene and graphene quantum dots: A review on synthesis and applications in energy, sensors and environment." ***Advances in Colloid and Interface Science***, 259 44-64(2018).

49. Yadav R., and Dixit C.K. "Synthesis, characterization and prospective applications of nitrogen-doped graphene: A short review." ***Journal of Science: Advanced Materials and Devices***, 2 141-149(2017).

50. Peng R., Li Y., Liu T., Si P., Feng J., Suhr J., and Ci L., "Boron-doped graphene coated Au@ SnO2 for high-performance trimethylamine gas detection." ***Materials Chemistry and Physics***, 239 121961(2020).

51. Rani P., Dubey G.S., and Jindal V.K., "DFT study of optical properties of pure and doped graphene." ***Physica E: Low-dimensional Systems and Nanostructures***, 62 28-35(2014).

52. Mirzaei M., Hadipour N.L., and Abolhassani M.R. "Influence of C-doping on the B-11 and N-14 quadrupole coupling constants in boron-nitride nanotubes: a DFT study." ***Zeitschrift für Naturforschung A***, 62 56-60(2007).

53. Mirzaei M., "Carbon doped boron phosphide nanotubes: a computational study." ***Journal of Molecular Modeling***, 17 89-96(2011).

54. Hulla J.E., Sahu S.C., Hayes A.W., "Nanotechnology: history and future", ***Human & Experimental Toxicology***, 34:1318-21(2015).

55. Saka R., Chella N., Nanotechnology for delivery of natural therapeutic substances: a review. ***Environmental Chemistry Letters***; 19:1097-106, (2021).

56. Shoukat R, and Khan MI., "Carbon nanotubes: a review on properties, synthesis methods and applications in micro and nanotechnology", ***Microsystem Technologies***, 27: 4183-4192, (2021).

57. Kyotani M., Goto H., Suda K., Nagai T., Matsui Y., and Akagi K., "Tubular-shaped Nano carbons prepared from polyaniline synthesized by a self-assembly process and their electrical conductivity", ***Journal of Nanoscience and Nanotechnology***, 8:1999-2004, (2008).

58. Wang J., Hu Z., Xu J., and Zhao Y., "Therapeutic applications of low-toxicity spherical Nano carbon materials", ***NPG Asia Materials***, 6:e 84,(2014).

59. Askins E.J., Zoric M.R., Li M., Luo Z., Amine K., and Glusac K.D., "Toward a mechanistic understanding of electro catalytic Nano carbon", ***Nature Communications***, 12:1-5(2021).

60. Schaub T.A., "Bottom-up synthesis of discrete conical Nano carbons". ***Angewandte Chime International Edition***, 59:4620-2(2020).

61. Zhang Q., Xie X.M., Wei S.Y., Zhu Z.Z., Zheng L.S., Xie S.Y., "The synthesis of conical carbon", ***Small Methods***, 5:2001086(2021).

62. Mirzaei M., "Silicon carbide Nano cones: computational analysis of chemical shielding's for pristine and boron/nitrogen decorated models", ***Super lattices and Microstructures***, 52:523-7(2012).

63. Hou T.Z., Chen X., Peng H.J., Huang J.Q., Li B.Q., Zhang Q., Li B., "Design principles for heteroatom-doped Nano carbon to achieve strong anchoring of polysulfide's for lithium–sulfur batteries", ***Small***, 12:3283-91(2016).

64. Ozkendir O.M., Cengiz E., Mirzaei M., Karahan I.H., Özdemir R., and Klysubun W., "Electronic structure study of the bimetallic Cu1-xZnx alloy thin films", ***Materials Technology***, 33:193-7(2018).

65. Xiao W., Jiang X., Liu X., Zhou W., Garba Z.N., Lawan I., Wang L, and Yuan Z., "Adsorption of organic dyes from wastewater by metal-doped porous carbon materials", ***Journal of Cleaner Production***, 284:124773(2021).

66. Khanvilkar M.B., Nikumbh A.K., Pawar R.A., Karale N.J., Nighot D.V., and Gugale G.S., "Synthesis and physicochemical properties of doped Nano oxides-dilute magnetic semiconductors". ***Journal of Materials Science: Materials in Electronics***, 30:13217-13229(2019).

67. Harismah K., Zohrevand B., Zandi H., "Computational investigating Fe-doped coronone surface for adsorption of hydrogen sulfide gaseous substance", ***Bio interface Research in Applied Chemistry***, 12:1651-59(2022).

68. Maiti S., Banerjee P., Purakayastha S., and Ghosh B., "Silicon-doped carbon semiconductor from rice husk char", ***Materials Chemistry and Physics***, 109:169-73(2008).

69. Yuan H., Li B., Zhu C., Xie Y., Jiang Y., and Chen Y., "Dielectric behavior of single iron atoms dispersed on nitrogen-doped Nano carbon", ***Applied Physics Letters***, 116:153101(2020).

70. Shaik S.A., Goswami A., Varma R.S., and Gawande M.B., "Nitrogen-doped Nano carbons (NNCs): current status and future opportunities", **Current Opinion in Green and Sustainable Chemistry**; 15:67-76(2019).

71. Liu X., Liu Y., Wang Y., Yuan D., Wang C., and Liu J., "Efficient electro sorption of uranium (VI) by B, N, and P co-doped porous carbon materials containing phosphate functional groups", ***Journal of Solid-State Electrochemistry***, 25:2443-54(2021).

72. Ammar H.Y., Eid K.M., and Badran H.M., "Interaction and detection of formaldehyde on pristine and doped boron nitride Nano-cage: DFT calculations", ***Materials Today Communications***, 25:101408(2020).

73. Goclon J., Bankiewicz B., Kolek P., and Winkler K., "Role of nitrogen doping in stoichiometric and defective carbon Nano-onions: structural diversity from DFT calculations", ***Carbon***, 176:198-208(2021).

74. Al-Haideri L.M., and Cakmak N., "Electronic and structural features of uranium-doped graphene: DFT study", ***Main Group Chemistry***, vol.21, no.1,pp 295-301(2022).

75. Ayoubi-Chianeh M., and Kassaee M.Z., "Detection of bendamustine anti-cancer drug via AlN and Si-doped C Nano cone and Nano sheet sensors by DFT", ***Structural Chemistry***, 31:2041-50(2020).

76. Yu X., and Raaen S., "Interaction between adsorbed hydrogen and potassium on a carbon Nano cone containing material as studied by photoemission", ***Journal of Applied Physics***, 118:105304(2015).

77. Mirzaei M., "Investigating pristine and carbon-decorated silicon Nano cones: DFT studies", ***Super lattices and Microstructures***, 58:130-4(2013).

78. EL-Barbary A.A., and Alkhateeb M.A., "DFT study of Se-doped Nano cones as highly efficient hydrogen storage carrier", ***Graphene***, 10:49-60(2021).

79. Haoyu L., and Karimi R., "Investigating a promising iron-doped graphene sensor for SO_2 gas: DFT calculations and QTAIM analysis", ***Main Group Chemistry***, vol.21, no.2, pp577-584,(2022).

80. Zarifi K., Rezaei F., and Seyed Alizadeh S.M., "A model of FeN -decorated BeO layer particle for CO gas adsorption", ***Main Group Chemistry***, vol. 21, no. 1, pp.125-132 (2022).

81. Mirzaei M., Hadipour N. L., and Abolhassani M. R., "Influence of C-doping on the B-11 and N-14 quadrupole coupling constants in boron-nitride nanotubes: a DFT study", ***Naturforsch***, 62a, 56 (2007).

82. Sherafati M., Rad A. S., Ardjmand M. and Heydarinasab A., “Beryllium oxide (BeO) nanotube provides excellent surface towards adenine adsorption: A dispersion-corrected DFT study in gas and water phases”, ***Current Applied Physics***, 18(9):1059–1065, (2018).

83. Rad A.S., Mirabi A., Peyravi M.,and Mirzaei M., “Nickel-decorated $B_{12}P_{12}$ nanoclusters as a strong adsorbent for SO_2 adsorption: Quantum chemical calculations”, ***Canadian Journal of Physics*** 95 (10), 958-962, (2017).

84. Yang Q., Li Z., Lu X., Duan Q., Huang L., and Bi J., “A review of soil heavy metal pollution from industrial and agricultural regions in China: Pollution and risk assessment”, ***Science of the total environment***, 642, 690-700, (2018).

85. Jacob J.M., Karthik C., Saratale R.G., Kumar S.S., Prabakar D., Kadirvelu K., and Pugazhendhi A., “Biological Approaches to Tackle Heavy Metal Pollution: A Survey of Literature”, ***Journal of Environmental Management***, 217: 56-70. (2018).

86. Ariaei Sh., Sakhaeinia H., Heydarinasab A., and Shokouhi M., “CO and NO selective adsorption by a $C_{16}Mg_8O_8$ Nano cage: A DFT Study”, ***Main Group Chemistry*** 20(4):1-11, (2021).

87. Dehaghani M.Z., Mashhadzadeh H.A., Salmankhani A., and Karami Z., “Fracture toughness and crack propagation behavior of nanoscale beryllium oxide graphene-like structures: A molecular dynamics simulation analysis”, ***Engineering Fracture Mechanics***, vol.235, 1077194 (2020).

88. Rostamiyan Y., Mohammadi V., and Mashhadzadeh A.H., “Mechanical, electronic and stability properties of multi-walled beryllium oxide nanotubes and Nano peapods: a density functional theory study”, ***Journal of Molecular Modeling*** 26(4), (2020).

89. Khodashenas B., Ardjmand M., Baei M. Sh., and Rad A., “Gelatin–Gold Nanoparticles as an Ideal Candidate for Curcumin Drug Delivery: Experimental and DFT Studies”, ***Journal of Inorganic and Organometallic Polymers and Materials***, 29:2186-2196(2019).

90. Ghazali F., Hosseini Sh., and Ketabi S., “DFT and Molecular Simulation Study of Gold Clusters as Effective Drug Delivery Systems for 5-Fluorouracil Anticancer Drug”, ***Journal of Cluster Science***, 34:1499-1509, (2022).

91. Tabandeh Z., and Reisi-Vanani A., "Investigation of the adsorption behavior of two anticancer drugs on the pristine and BN-doped graphdiyne Nano sheet: A DFT-D3 perception", ***Diamond and Related Materials,*** 119(28):108564, (2021).

92. Derdare M., Boudjahem Abd-G., Boulbazine M., "Adsorption of the NO_2, N_2O and NH_3 molecules over the C_20 and MC_{19} (M = Ru, Ir and Au) clusters: A DFT approach", ***Surfaces and Interfaces***, Volume 24:101114, (2021).

93. Derdare M., Boudjahem Abd-G., Boulbazine M., "Adsorption and decomposition mechanism of N_2O molecule over MC_{23} (M = Ru, Mn, V, Pd, and Rh) Nanoclusters: A comparative DFT investigation", ***Structural Chemistry***, 33:2043–2062(2022).

94. Shyma M.Y., Sheena M. Y., and Ullah Z., **"**Computational Study of Sorbic Acid Drug Adsorption onto Coronene / Fullerene/ Fullerene-Like $X_{12}Y_{12}$ (X = Al, B and Y = N, P) Nano cages: DFT and Molecular Docking Investigations", ***Journal of Cluster Science***, v.33, no.4, pp.1809 – 1819, (2022).

95. Padash R, Esfahani M. R., and Rad A., "The Computational Quantum Mechanical Study of Sulfamide Drug Adsorption onto $X_{12}Y_{12}$ Fullerene-like Nano cages: Detailed DFT and QTAIM investigations", ***Journal of bio molecular Structure & Dynamics***, vol. 39, issue 15, (2020).

96. Derakhshandeh M., "BC_{l3} Adsorption on Pristine, S-Doped, and Cr-Doped Graphynes: A DFT Study", ***Research Square,*** DOI:10.21203/rs.3.rs-512555/v1(2021).

97. Abbasi M., and Nemati-Kande E., "Enhancing the reactivity of carbon-nanotube for carbon monoxide detection by mono- and co-doping of boron and nitrogen heteroatoms: A DFT and TD-DFT study", ***Journal of Physics and Chemistry of Solids***, 158:110230, (2021).

98. Wang M., Cheng S., Zeng W., and Zeng Q., "Adsorption of toxic and harmful gas CO on TM (Ni, Pd, Pt) doped MoTe2 monolayer: A DFT study", ***Surfaces and Interfaces***, vol. 31, 102111, (2022).

99. Al-Saadi B., "Studying the physical properties of (X2GdIn(X=Au, Cu, Au)", ***Ph.D. thesis, University of Setif, Algeria***, (2013).

100. Kireev P., “La physique des semiconductors”, ***2 éme édition***, ***Edition Mir Moscou***, 6v(1975).

101. Born M., and Oppenheimer R.J., “On the quantum Theory of Molecules”, ***Ann. phys.***, 84, 457, (1927).

102. Ibrahim Gh. A., “Structural and optical study of quinoxaline Using the density functional theory”, ***M.Sc. thesis. University of Shaheed Hama Lakhdar, Al Wadi, Algeria***, (2021).

103. Hartree, D.R., “The Wave Mechanics of an Atom with a Non-Coulomb Central Field. Part I. Theory and Methods”, ***Mathematical Proceedings of the Cambridge Philosophical Society***, 24, 89-110, http://dx.doi.org/10.1017/S0305004100011919(1928).

104. Hartree D.R., “The calculation of atomic structures”, ***John Wiley and Sons***, New York. p376, (1957).

105. Fock V., “On a possible geometric interpretation of relativistic quantum theory”, ***Z.physic*** (***Zeitschrift für Physik***), 61,126(1920).

106. Slater J.C., “Atomic shielding constants”, ***Phys. Rev.*** 35, 210(1930).

107. Halima Z., “Study of the structural and electronic properties of a compound of interest in nonlinear optics”, ***M.Sc. thesis, University of M'sila, Algeria***, (2017).

108. Kohn W., and Sham L.J., “Self-consistent Equations Including Exchange and Correlation Effects”, ***physics Review,*** 140, A1133 (1965).

109. Cohen M.H., Frydel D., Bruke K., and Engel E., “Total energy density as an interpretative tool”, ***J. Chem. Physics,*** Vol.113, No. 8, pp. 2990-2994, (2000).

110. Thomas L.H., “The Calculation of Atomic Fields”, ***Mathematical Proceedings of the Cambridge Philosophical Society***, 23, pp. 542-548, (1927).

111. Fermi E., “Un Metodo Statistico per la Determinazione di alcune Prioprietà dell'Atomo (A Statistical Method for the Determination of the Priority of the Atom)”, ***Accademia Nazionale dei Lincei,*** 6: 602–607, (1927).

112. Hohenberg P.C., and Kohn W. “Inhomogeneous Electron Gas”, ***physics Rev.*** B. 136.864(1964).

113. Zawazi M. R., “Structural and spectroscopic study of dichloromethylaniline using Density Function Theory”, ***M.Sc. thesis, Al-Wadi University, Algeria***, (2019).

114. Benmakhlof A., “Simulation des propriétés optiques, électroniques, Magnétiques et streucturales des matériaux semiconducteurs et/ou métallique”, ***Thése de doctorat, université de Bejaia, (***2017).

115. Cottenier S. “Density Functional theory and the family of (L) APW-methods: A step-by-step introduction”, ***https://www.researchgate.net/publication/228397838***, (2004).

116. Perdew J., and Wang W., “Density-functional thermochemistry. The effect of the Perdew-Wang generalized-gradient correlation correction”, ***Physics Rev.*** **B**, 45, 244(1992).

117. Perdew J.P., Burke S. and Ernzerhof M., “Generalized Gradient Approximation Made Simple”, ***Physics Rev.Let.***77:3865, (1996).

118. Wu Z., and Cohen R.E. “More accurate generalized gradient approximation for solids”, ***Physics Rev.*** B, 73: 235116, (2006).

119. Dirac P.A., “Note on Exchange Phenomena in the Thomas Atom”, ***Mathematical Proceedings of the Cambridge Philosophical Society***, 26, 376-385, (1930).

120. Harris J., and Jones R.O., “The surface energy of a bounded electron gas”, ***Journal of Physics F: Metal Physics***, 4: 1170, (1974).

121. Becke A.D., and Chem J., “A new mixing of Hartree-Fock and local density functional theories”, ***phys.,*** 98:1372, (1993).

122. Becke A.D., and Chem J., “Density-functional thermochemistry. The role of exact exchange”, ***physics,*** 98:5648, (1993).

123. Abdelmadjid K., “Etude par DFT et TD-DFT de la structure et des propriétés optiques de quelques complexes de métaux de transition (Study by DFT and TD-

DFT of the structure and optical properties of some complexes of transition metals)", ***mémoire de magister, université de Constantine, Algeria***, (2010).

124. Young D., "Computational Chemistry: A Practical Guide for Applying Techniques to Real World Problems", ***John Wiley & Sons, inc: USA***, (2001).

125. Jensen, F., "Introduction to computational Chemistry", ***2nd ed.; John Wiley and Sons, inc: England***, (2007).

126. Matczak P., "Assessment of B3LYP combined with various ECP basis sets for systems containing Pd, Sn, and Pb", ***Computational and Theoretical Chemistry*** 983:25–30,(2012).

127. Frisch M. J., Trucks G.W., Schlegel H.B., Scuseria G.E., Robb M.A., Cheeseman J.R., Scalmani G., Barone V., Mennucci B., Petersson G.A., Nakatsuji H., Caricato M., Li X., Hratchian H.P., Izmaylov A.F., Bloino J., Zheng G., Foresman B., Ortiz J.V., Cioslowski J., and Fox D.J., "Gaussian 09, Revision A.02", ***Gaussian Inc. Wallingford, CT***, (2009)

128. Bodaghi A., Mirzaei M., Seif A., and Giahi M., "A computational NMR study on zigzag aluminum nitride nanotubes", ***Physica E: Low-dimensional Systems and Nanostructures*** Volume 41, Issue 2, Pages 209-212, (2008).

129. Fallahpour F., and Ariaei S., "Computational investigation of B6 particle for H2S capturing", ***Advanced Journal of Science and Engineering***, 2:31-35, (2021).

130. Gilani A.G., Taghvaei V., Rufchahi E.M., Mirzaei M., "Photo-physical and structural studies of some synthesized arylazoquinoline dyes", ***Spectrochimica Acta Part A: Molecular and Bimolecular Spectroscopy*** 185, 111-124, (2017).

131. Blanco M.A., Martín Pendás A., Francisco E., "Interacting quantum atoms: a correlated energy decomposition scheme based on the quantum theory of atoms in molecules", ***Journal of Chemical Theory and Computation***, 1:1096-109, (2005).

132. Zax D.B., Bielecki A., Zilm K.W., Pines A., and Weitekamp D., "Zero field NMR and NQR", ***The Journal of Chemical Physics***, 83:4877-905, (1985).

133. Verma P., and Truhlar D.G., Status and challenges of density functional theory. ***Trends in Chemistry***, 2:302-18, (2020).

134. Chiodo S., Russo N., and Sicilia E., "LANL2DZ basis sets recontacted in the framework of density functional theory", ***The Journal of Chemical Physics***, 125:104107, (2006).

135. Bagheri Z., Mirzaei M., Hadipour N.L., Abolhassani M.R., "Density functional theory study of boron nitride nanotubes: calculations of the N-14 and B-11 nuclear quadrupole resonance parameters", ***Journal of Computational and Theoretical Nanoscience***, 5:614-8, (2008).

136. Moon J., Huang Z,, Wu W. and Oh S., "Pb-doped *p*-type Bi_2Se_3 thin films via interfacial engineering", ***Phys. Rev. Mater***,4, 024203, (2020).

137. Ranjan P., Kumar P., Chakraborty T., Sharma M., and Sharma S., "A study of structure and electronic properties of chalcopyrite's semiconductor invoking density functional theory", ***Materials Chemistry and Physics***, 241, 122346, (2020).

138. Mirzaei M., Rasouli A.H., Saedi A. "HOMO-LUMO photosensitization analyses of coronene-cytosine complexes". ***Main Group Chemistry***, vol. 20 no. 4 pp. 565-573 (2021).

139. Zare A., Mirzaei M., Rostami M., and Jafari E. "Photosensitization of phthalocyanine for singlet oxygen generation in photodynamic therapy applications", ***Journal of Medicinal and Chemical Sciences*** 3: 55-59, (2020).

140. Günaydın S., Alcan V., Mirzaei M., and Ozkendir O.M., "Electronic structure study of Fe substituted RuO_2 semiconductor", ***Lab-in-Silica***, 1(1), 7–10, (2020).

141. Zahedi H., Yousefi M., and Mirzaei M., "DFT investigation of AlP-doped BN nanotube for CO gas capturing". ***Lab-in-Silica***, 1: 38-43, (2020).

142. Ozkendir O.M., "Electronic structure study of Sn-substituted InP semiconductor", ***Advanced Journal of Science and Engineering***, 1: 7-11, (2020).

RESUME

Lina Majeed Hayder AL-HAIDERI she graduated from primary and secondary education in this city. She completed his secondary education at Al-Karkh Secondary School, and after that, she started his bachelor's program in the Department of Physics at the University of Baghdad in 2001. Then, she obtained a master’s degree in physics/molecular physics in 2005, and she started teaching as an assistant lecturer at the University of Baghdad, and she is still working there. She was promoted to a lecturer in 2013. She was accepted into Karabük University to complete her PhD in the same field.